CHAPTER: 3 Ternary binuclear complexes.

3.1 Introduction

3.2 Experimental

3.3 Results and Discussion

3.4 References

3.1 Introduction

The growing interest in the study of binuclear copper (II) complexes is due to their probable role as potential models for several important biological systems, containing binuclear spin coupled sites [1-3]. These binuclear copper (II) complexes can be used as enzyme catalysts in several biochemical reactions [4]. The catalytic activity of these complexes can be attributed to their redox and magnetic characteristics and hence, it is worth considering the factors that affect the electron transfer or spin exchange between two metal centers. Unlike complexes with single atom bridge where direct super exchange can take place, polyatomic bridging units function in a more complex manner. Study of complexes with different geometries around the metal ion and with binucleating ligands possessing σ and π – orbitals have indicated that the extent of spin exchange in such compounds depends on the energy of the magnetic orbitals and the symmetry of the metal environment [5-11]. These can be affected by change in nucleophilicity and the geometry of the ligands, respectively. The coordination geometry and energy of the metal ions can be affected by the non-bridging part of the ligands and they can affect the magnetic exchange.

Binuclear complexes with oxalate [12], squarate [12], dihydroxybenzoquinone [13], naphthazarin [14] and quinizarin bridges have been reported. 2,5-Penta and hexa coordinated complexes of the last two compounds were shown not to undergo any magnetic exchange interaction because ligand orbitals with proper symmetry are absent [14,15].

The ferromagnetic property in the complexes developed due to either accidental or due to the strict orthogonality of their magnetic orbitals and / or to spin polarization effects. Ferromagnetic interaction between copper (II) centers bridged by planar phthalato aromatic ligand provided similar environment to the metal centers [16]. Copper (II) complexes of binucleating ligands with two bidentate sites separated by aromatic rings have been studied earlier [17]. In such complexes spin exchange between two metal centers propagated through π delocalized bridge. However, no work has been carried out on ternary binuclear Schiff base complexes with substituted

binuclear Schiff base ligand forming a bridge and the metal ions coordinated to another bidentate ligand.

In the present study an attempt is made to synthesize the binuclear complexes of copper (II) and to study the magnetic exchange at variable temperature through long aromatic bridging groups, the change of electronic environment around the metal centers was also studied by changing the non coordinating part of the ligands. Molecular modelling by force field calculation has been used to work out the geometrical parameters in various complexes and they have been correlated with magnetic property.

In order to achieve the above goal, ternary complexes possessing a tertiary diimine, 2,2'-bipyridine or 1,10-phenanthroline as a primary ligand and 2-hydroxybenzaldehyde, 2-hydroxynaphthaldehyde or 2-hydroxy-3-methoxybenzaldehyde as secondary ligand, have been synthesized. These mononuclear complexes have been used as precursors to synthesize ternary binuclear complexes by condensation with 4,4'-diaminodiphenylmethane, 4,4'-diaminodiphenylether, 4,4'-diaminodiphenylsulphone or 3,3'-diaminodiphenylsulphone. The ternary binuclear complexes have been characterized by elemental analysis, conductance, spectral and magnetic properties in 90K to 300K temperature range. On the basis of these experimental results long range spin exchange interaction between two copper centers have been studied and correlated with variation in non bridging part of the ligands.

3.2. Experimental

3.2.1 Chemicals:

1,10-phenanthroline, 2,2'-bipyridine, and sodium perchlorate of AR grade were procured from Merck and were used without further purification. All other chemicals were as described earlier in chapter 2.

3.2.2 Physical measurements:

Elemental analyses of the complexes were done as described in chapter 2.

Specific conductivity of all the complexes in DMF solution having 1.0 mmolar concentration was measured using a Toshniwal conductivity bridge.

The electronic spectra of the complexes in UV-VIS region were recorded in methanolic solutions using Shimadzu UV-240 and Perkin Elmer Lambda 35, UV – VIS spectrophotometer.

IR spectra (as KBr pellets) were recorded on Perkin Elamer FT-IR, spectrum RXI and Perkin Elmer FT-IR, spectrum GX spectrometer.

The ESR spectra of the complexes $[Cu_2(bipy)_2naphDPM](ClO_4)_2$, $[Cu_2(bipy)_2vanDPM](ClO_4)_2$, $[Cu_2(bipy)_2van4\text{-}DPS](ClO_4)_2$ and $[Cu_2(bipy)2van3\text{-}DPS](ClO_4)_2$ were recorded at RT and liquid nitrogen temperature on a Varian E-15 spectrometer. The ESR spectra of the complexes $[Cu_2(phen)_2salDPM](ClO_4)_2$, $[Cu_2(phen)_2salDPE](ClO_4)_2$, $[Cu_2(bipy)_2salDPM](ClO_4)_2$ and $[Cu_2(bipy)_2salDPE](ClO_4)_2$ were recorded at room temperature on a Brucker instrument.

The FAB mass spectrum of the complexes were recorded at room temperature as detailed earlier in chapter 2.

Magnetic Susceptibility of the complexes was measured with polycrystalline samples in the 90 – 300 K temperature range using a Faraday set up as detailed earlier in chapter 2. The measurements were made at a field strength of 0.8 tesla at 44.2 AMPs. Temperature was measured and controlled using OMEGA CYC 3200, Autotunning Temperature Controller having an accuracy of 0.01°. 15mg to 20 mg of sample was used for the measurements. Diamagnetic corrections were incorporated using Pascal's constants.

3.3.1 Synthesis of ternary mononuclear complexes, $[Cu(phen)sal]ClO_4$:

A warm solution containing equimolar amounts of 1,10-phenanthroline (1.984 g, 10 mmol) and 2-hydroxybenzaldehyde (1.221 g (≈ 1.10 ml), 10 mmol) in 40 ml ethyl alcohol was added to a warm solution of 1.997 g. (10 mmol) copper acetate

monohydrate in 30 – 40 ml water. The resulting solution was refluxed on water bath for about 15 minutes. To this was added drop wise a concentrated solution of sodium perchlorate in water till the precipitation was complete [Caution: The perchlorate salts are known to be highly explosive]. The resulting solid was filtered, washed with 30 ml (7-8 portions) water alcohol mixture followed by 15 ml CH_3OH and dried in air.

Other ternary mononuclear complexes, [Cu(bipy)sal]ClO_4, [Cu(phen)naph]ClO_4, [Cu(bipy)naph]ClO_4, [Cu(phen)van]ClO_4 and [Cu(bipy)van]ClO_4 were synthesized by using the above procedure and appropriate quantity of tertiary diamines, 2-hydroxyaromatic aldehydes, copper acetate monohydrate and sodium pechlorate, **Scheme 3.1.**

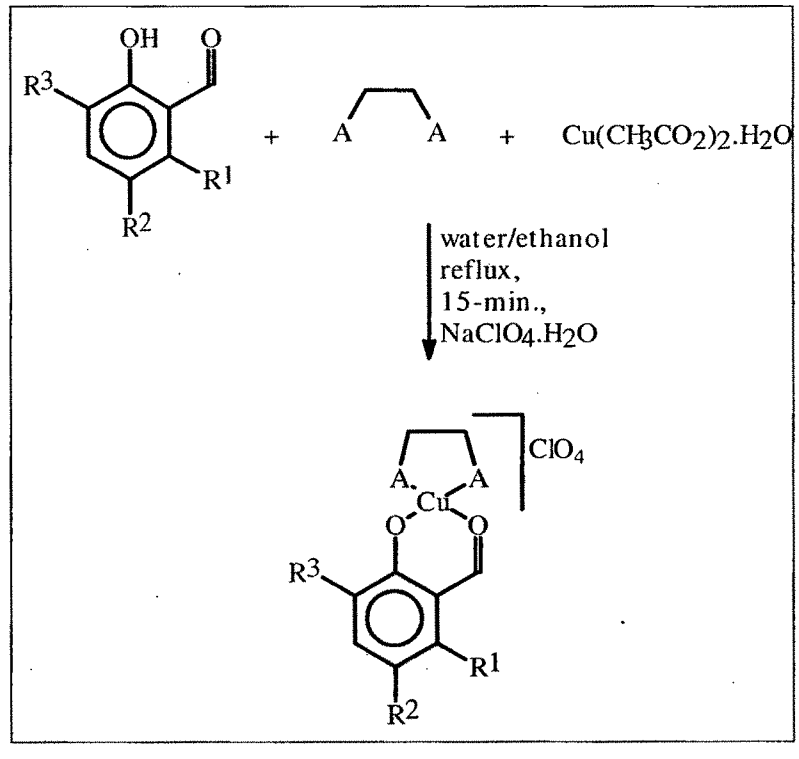

Scheme 3.1. Synthesis of ternary mononuclear complexes.

3.3.2 Synthesis of binuclear complexes, $[Cu_2(phen)_2salDPM](ClO4)_2$:

0.8 mmol (0.387 g) of the ternary complex $[Cu(phen)sal](ClO_4)$ was dissolved in 20 ml of methanol and to this 0.4 mmol (0.825 g) of 4,4'-diaminodiphenyl methane dissolved in 20 ml of methanol was added drop wise over 30 minutes. The reaction mixture was allowed to reflux for 11 hours. Consumption of 4,4'-diaminodiphenyl methane was monitored by TLC. At the end of this period a brown coloured compound was separated. It was cooled and the solid obtained was washed thoroughly with 25 ml methanol in 5-6 portions and dried in air at ~ 80 °C.

Complexes **(3-II – 3-XIX)** were synthesized by using the above procedure and appropriate quantity of ternary complexes and respective diamines, **Scheme 3.2.** The results of the C, H and N analyses, refluxing time for each complexes and conductivity measurements have been given in **Table 3.1.**

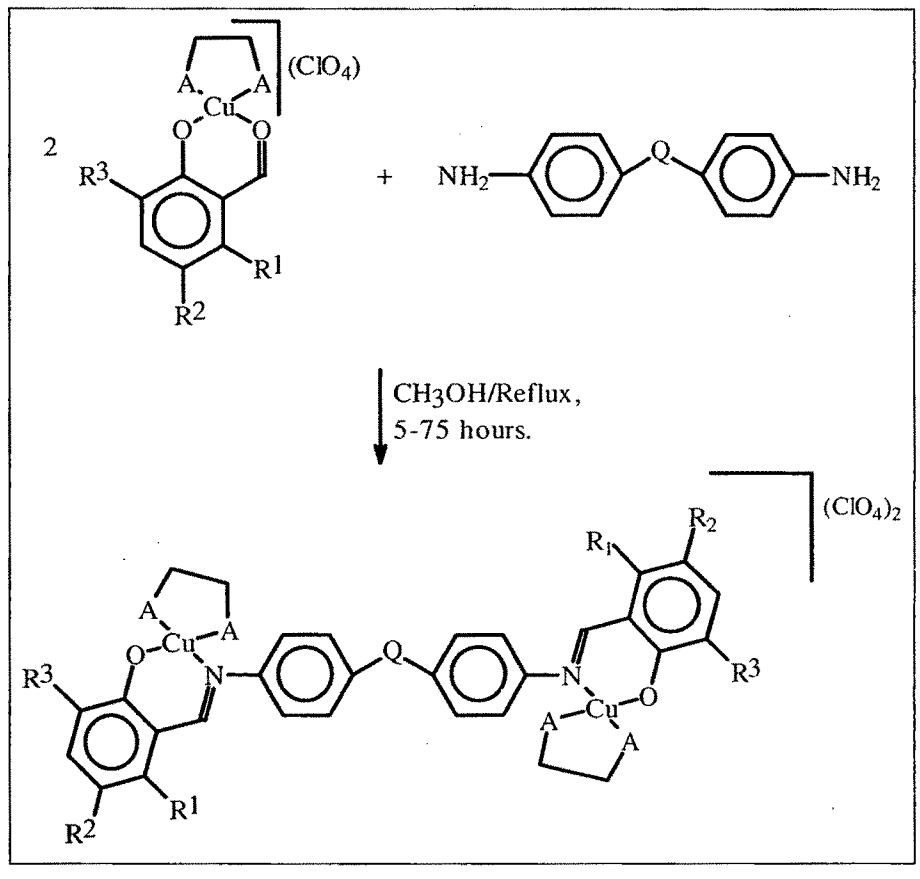

3-I, 3-II, 3-III, 3-IV: R^1 = H, R^2 =H, R^3 = H.

3-V, 3-VI, 3-VII, 3-VIII, 3-IX, 3-X, 3-XI: R^1R^2 = -$(CH=CH)_2$-, R^3 = H.

3-XII, 3-XIII, 3-XIV, 3-XV, 3-XVI, 3-XVII, 3-VIII, 3-XIX: R^1 = H, R^2 =H, R^3 = -OCH_3.

3-I, 3-II, 3-V, 3-VI, 3-VII, 3-VIII, 3-XII, 3-XIII, 3-XIV, 3-XV: AA = 1,10-phen.

3-III, 3-IV, 3-IX, 3-X, 3-XI, 3-XVI, 3-XVII, 3-XVIII, 3-XIX: AA = 2,2'-bipy.

3-I, 3-III, 3-V, 3-IX, 3-XII, 3-XVI: Q = -CH_2-

3-II, 3-IV, 3-VI, 3-X, 3-XIII, 3-XVII: Q = -O-

3-VII, 3-XIV, 3-XVIII: Q = -SO_2- (4,4')

3-VIII, 3-XI, 3-XV, 3-XIX: Q = -SO_2- (3,3')

Scheme 3.2

(Binuclear complexes **3- I** to **3-XIX)**

3.3 Result and discussion:

The reactions of presynthesized binucleating Schiff base ligands, (H_2L^{1a}, H_2L^{1b}, H_2L^{1d}, H_2L^{2a}, H_2L^{2d}, H_2L^{3a}, H_2L^{3d}, H_2L^{4a}, and H_2L^{4d}) with cupric acetate monohydrate and the bidentate tertiary diamines (AA) i.e. 2,2'-bipyridine and 1,10-phenanthroline, generally, resulted in the formation of binuclear, $[Cu_2L_2]$, complexes as reported in chapter 2 and $[CuAA]^{2+}$ complexes. Hence, it was necessary to plan a different strategy for the synthesis of desired ternary binuclear complexes with a single bridging ligand (**Scheme 3.1**). The formation of ternary $[CuAA(B)](ClO_4)_2$ complexes where AA is tertiary diamine viz. bipy & phen and B is a 2-hydroxyaromatic carbonyl viz. 2-hydroxybenzaldehyde(sal), 2-hydroxynapthaldehyde (naph) and 2-hydroxy-3-methoxybenzaldehyde (van) can be achieved with high purity by allowing equimolar amounts of the metal ion and the two ligands between pH 5.5 – 6.5 in 50% ethanol water media. It has been proved [18] that the formation of the above type of ternary copper (II) complexes with a tertiary diamine and a O O coordinating bidentate ligand is maximum, 80 – 90% with very small amounts of the binary species. Thus the ternary complex can be synthesized with high purity by use of an appropriate anion like perchlorate in this case.

The coordination of carbonyl O in sal, naph or van with copper ion makes carbonyl carbon more electrons deficient. The presence of a π – acidic ligand with metal ion further reduces the electron density over the carbonyl group and thus it becomes an easier target for the attack of an aromatic amine. Thus, the reactions of the ternary complexes with aromatic diamines viz. 4,4'-diaminodiphenylmethane, 4,4'-diaminodiphenylether, 4,4'-diaminodiphenylsulphone and 3,3'-diaminodiphenylsulphone resulted in the formation of the desired ternary binuclear complexes with good yields.

The values of elemental analyses of complexes are agreeable with the suggested molecular formulae, as ternary binuclear complexes (**Table 3.1**). The complexes are found highly soluble in DMF. The conductivity measurements were

carried out in DMF. All the nineteen complexes have molar conductivity values between 130 – 165 ($\Omega^{-1}M^{-1}cm^2$) which correspond to 1:2 electrolytes. This confirms the presence of two perchlorates in each complex and their ionic character. The analytical data indicate the presence two water molecules in complexes, **3-V, 3-VI, 3-VII, 3-VIII, 3-X, 3-XI, 3-XIII, 3-XIV** and **3-XV.** However, thermal analysis could not be carried out for the confirmation of nature of water molecules because of the presence of perchlorates ion. The presence of water molecules is confirmed only by IR spectra.

Table 3.1: Reflux time, yields, elemental analysis and Molar conductivity of the ternary binuclear complexes.

Comp. No	Complexes	Reflux time (hours)	Yields (%)	Elemental analysis Obsd. (Calc.[a])			Molar conductivity[b] ($\Omega^{-1}M^{-1}cm^2$)
				C	H	N	
3- I	$[Cu_2(phen)_2salDPM](ClO_4)_2$	11	77	56.34	3.25	7.75	140.28
	$C_{51}H_{36}O_{10}N_6Cl_2Cu_2$			(56.14)	(3.30)	(7.71)	
3 -II	$[Cu_2(phen)_2salDPE](ClO_4)_2$	11	83	54.76	3.09	7.64	140.14
	$C_{51}H_{34}O_{11}N_6Cl_2Cu_2$			(54.94)	(3.11)	(7.69)	
3-III	$[Cu_2(bipy)_2salDPM](ClO_4)_2$	11	81	54.38	3.37	7.92	140.14
	$C_{47}H_{36}O_{10}N_6Cl_2Cu_2$			(54.12)	(3.45)	(8.06)	
3-IV	$[Cu_2(bipy)_2salDPE](ClO_4)_2$	17	64	52.78	3.13	7.87	140.14
	$C_{47}H_{34}O_{11}N_6Cl_2Cu_2$			(52.87)	(3.25)	(8.04)	
3-V	$[Cu_2(phen)_2naphDPM](ClO_4)_2.2H_2O$	21	42	57.28	3.17	5.60	138.30
	$C_{59}H_{44}O_{12}N_6Cl_2Cu_2$			(57.74)	(3.58)	(6.85)	
3-VI	$[Cu_2(phen)_2naphDPE](ClO_4)_2.2H_2O$	16	65	56.49	3.03	6.00	160.16
	$C_{58}H_{42}O_{13}N_6Cl_2Cu_2$			(56.67)	(3.42)	(6.83)	
3-VII	$[Cu_2(phen)_2naph4$-	35	66	54.65	2.96	5.61	160.16
	$DPS](ClO_4)_2.2H_2O$			(54.54)	(3.28)	(6.58)	
	$C_{58}H_{42}O_{14}N_6Cl_2SCu_2$						

Continued.....

Comp. No	Complexes	Reflux time (hours)	Yields (%)	Elemental analysis Obsd. (Calc.[a]) C	H	N	Molar conductivity[b] ($\Omega^{-1}M^{-1}cm^2$)
3-VIII	$[Cu_2(phen)_2naph3\text{-}DPS](ClO_4)_2.2H_2O$	75	57	54.18	3.18	5.39	160.16
	$C_{58}H_{42}O_{14}N_6Cl_2SCu_2$			(54.54)	(3.28)	(6.58)	
3-IX	$[Cu_2(bipy)_2naphDPM](ClO_4)_2$	15	49	57.82	3.39	6.91	135.29
	$C_{55}H_{40}O_{10}N_6Cl_2Cu_2$			(57.78)	(3.50)	(7.35)	
3-X	$[Cu_2(bipy)_2naphDPE](ClO_4)_2.2H_2O$	16	60	55.54	3.19	6.63	140.14
	$C_{54}H_{42}O_{13}N_6Cl_2Cu_2$			(54.91)	(3.55)	(7.11)	
3-XI	$[Cu_2(bipy)_2naph3\text{-}DPS](ClO_4)_2.2H_2O$	72	60	52.38	3.25	6.03	165.16
	$C_{54}H_{42}O_{14}N_6Cl_2SCu_2$			(52.76)	(3.47)	(6.83)	
3-XII	$[Cu_2(phen)_2vanDPM](ClO_4)_2$	15	72	54.41	3.47	6.49	130.26
	$C_{53}H_{40}O_{12}N_6Cl_2Cu_2$			(55.30)	(3.47)	(7.30)	
3-XIII	$[Cu_2(phen)_2vanDPE](ClO_4)_2.2H_2O$	6	79	52.93	3.11	6.60	135.01
	$C_{52}H_{42}O_{15}N_6Cl_2Cu_2$			(52.52)	(3.53)	(7.07)	
3-XIV	$[Cu_2(phen)_2van4\text{-}DPS](ClO_4)_2.2H_2O$	26	60	49.21	3.24	5.68	160.01
	$C_{52}H_{42}O_{16}N_6Cl_2SCu_2$			(50.48)	(3.39)	(6.79)	

Continued....

Comp. No	Complexes	Reflux time (hours)	Yields (%)	Elemental analysis Obsd. (Calc.[a])			Molar conductivity[b]
				C	H	N	($\Omega^{-1}M^{-1}cm^2$)
3-XV	$[Cu_2(phen)_2van3\text{-}DPS](ClO_4)_2.2H_2O$	31	67	49.28	3.12	5.39	165.16
	$C_{52}H_{42}O_{16}N_6Cl_2SCu_2$			(50.48)	(3.39)	(6.79)	
3-XVI	$[Cu_2(bipy)_2vanDPM](ClO4)_2$	13	84	53.22	3.48	7.20	150.15
	$C_{49}H_{40}O_{12}N_6Cl_2Cu_2$			(53.35)	(3.63)	(7.62)	
3XVII	$[Cu_2(bipy)_2vanDPE](ClO4)_2$	5	90	52.29	3.23	7.23	130.13
	$C_{48}H_{38}O_{13}N_6Cl_2Cu_2$			(52.17)	(3.44)	(7.60)	
3-XVIII	$[Cu_2(bipy)_2van4\text{-}DPS](ClO_4)_2$	58	29	49.98	3.60	7.32	130.13
	$C_{48}H_{38}O_{14}N_6Cl_2SCu_2$			(49.99)	(3.29)	(7.29)	
3-XIX	$[Cu_2(bipy)_2van3\text{-}DPS](ClO_4)_2$	23	59	49.77	3.15	7.43	140.14
	$C_{48}H_{38}O_{14}N_6Cl_2SCu_2$			(49.99)	(3.29)	(7.29)	

[a] The values in parenthesis are theoretical values calculated from the molecular formulae.

[b] The conductivity measurements were carried out with 1×10^{-3} M solution of the complexes in DMF.

3.3.1 Electronic spectra:

The electronic spectra of the complexes have been recorded both in methanolic solutions and diffuse reflectance in the solid state (**Table 3.2**).

The complexes have strong absorptions between 280 – 300 nm and between 388 –406 nm. The former can be attributed to the $\pi \rightarrow \pi^*$ transitions within the ligands. The strong absorption at $\approx$ 390 nm is due to the metal to ligand charge transfer transition in the complexes. The ligand field transitions are observed in the diffuse reflectance spectra as broad bands with low intensity. The broad band can be attributed to a combination of $^2A_{1g} \leftarrow {}^2B_{1g}$, $^2B_2g \leftarrow {}^2B_{1g}$ and $^2E_{1g} \leftarrow {}^2B_{1g}$ transitions in a d^9 metal ion.

In presence of electron delocalization between two copper (II) ions, there can be mixing of metal centered molecular orbitals and more number of closely spaced orbitals can result. This can make the ligand field band broader in the binuclear copper (II) complexes as is observed in the present case.

Table 3.2: Electronic spectral data of ternary binuclear complexes.

Comp. No.	Complexes	Intra ligand and CT trans. (λ in nm)	d-d transition (λ in nm)
3-I	$[Cu_2(phen)_2salDPM](ClO_4)_2$	294, 350, 392	782*
3-II	$[Cu_2(phen)_2salDPE](ClO_4)_2$	293, 350, 389	738*
3-III	$[Cu_2(bipy)_2salDPM](ClO_4)_2$	276, 308, 390	776*
3-IV	$[Cu_2(bipy)_2salDPE](ClO_4)_2$	298, 310, 388	762*
3-V	$[Cu_2(phen)_2naphDPM](ClO_4)_2.2H_2O$	296, 314, 388	726*
3-VI	$[Cu_2(phen)_2naphDPE](ClO_4)_2.2H_2O$	282, 306, 398	618
3-VII	$[Cu_2(phen)_2naph4\text{-}DPS](ClO_4)_2.2H_2O$	294, 315, 406	618
3-VIII	$[Cu_2(phen)_2naph3\text{-}DPS](ClO_4)_2.2H_2O$	288, 314, 380	617
3-IX	$[Cu_2(bipy)_2naphDPM](ClO_4)_2$	286, 300, 404	630
3-X	$[Cu_2(bipy)_2naphDPE](ClO_4)_2.2H_2O$	290, 300, 396	635
3-XI	$[Cu_2(bipy)_2naph3\text{-}DPS](ClO_4)_2.2H_2O$	292, 315, 388	606
3-XII	$[Cu_2(phen)_2vanDPM](ClO_4)_2$	282, 348, 390	654
3-XIII	$[Cu_2(phen)_2vanDPE](ClO_4)_2.2H_2O$	286, 310, 390	652
3-XIV	$[Cu_2(phen)_2van4\text{-}DPS](ClO_4)_2.2H_2O$	284, 334, 400	635
3-XV	$[Cu_2(phen)_2van3\text{-}DPS](ClO_4)_2.2H_2O$	284, 332, 400	634
3-XVI	$[Cu_2(bipy)_2vanDPM](ClO_4)_2$	284, 300, 390	634
3-XVII	$[Cu_2(bipy)_2vanDPE](ClO_4)_2$	286, 300, 392	629
3-XVIII	$[Cu_2(bipy)_2van4\text{-}DPS](ClO_4)_2$	288, 300, 400,	620
3-XIX	$[Cu_2(bipy)_2van3\text{-}DPS](ClO_4)_2$	286, 300, 396	624

* The ligand field absorptions in the complexes with* are observed in d. r. s. All other values in methanolic solutions.

3.3.2 Infra red Spectra:

The IR spectra of the complexes in the region 400 – 4000 cm^{-1} are very rich and consist of the vibrational excitations in both ligands and perchlorate. The observation of these bands, shifts in the bands corresponding to the functional groups involved in coordination and the presence of M-L skeletal vibrations make them agreeable with the proposed structures. The absorption frequency of the stretching in imine >C=N appears between 1600 – 1616 cm^{-1}. These are at lower energies compared to the free organic Schiff base ligands, which is 1630 – 1660 cm^{-1}. The shift in the $\nu_{>C=N}$ (imine) towards lower energy in the complexes indicates that the imine nitrogen is involved in coordination with the Cu(II) ion. The IR spectra of the complexes exhibit a broad and strong band about 1086 – 1108 cm^{-1} without any splitting corresponding to the characteristic asymmetric stretching vibration in non – coordinated ClO_4^-, [19].

Moreover, complexes **3-I, 3-III, 3-V, 3-IX** and **3-XII** and **3-XVI** exhibiting bands due to asymmetric stretching around 2920 cm^{-1} indicate the presence of $-CH_2-$ group. Complexes **3-II, 3-IV, 3-VI, 3-X, 3-XIII** and **3-XVII** have absorption due to showing the stretching in C-O-C, ν_{as}-O-, around - 1250 cm^{-1} indicating the presence of –O- group. The complexes, **3-VII, 3-VIII, 3-XI, 3-XIV, 3-XV, 3-XVIII** and **3-XIX** have absorptions correspond to ν_{-SO2-}(s) between 1140 - 1149 cm^{-1} and ν_{-SO2-}(as) between 1301 to 1338 cm^{-1} supporting the presence of $-SO_2-$ group in the complexes. Presence of absorption frequencies for $-CH_2-$, –O- and $-SO_2-$ groups indicated their presence in the bridging group. Complexes **3-XII** to **3-XIX**, exhibiting symmetric frequency in 1033 to 1062 cm^{-1} and asymmetric frequency at 1250 cm^{-1} corresponding to the C-O-CH_3 group.

Complexes **3-V, 3-VI, 3-VII, 3-VIII, 3-X, 3-XI, 3-XIII, 3-XIV** and **3-XV** show a broad band between 3436 to 3538 cm^{-1}, which can be attributed to the presence of lattice held water molecules. All the complexes exhibit absorptions at 3055 – 3084 cm^{-1} corresponding to aromatic –C-H stretching, (**Table 3.3**, **Fig. 3.2.1** to **Fig. 3.4.8**).

Table 3.3: IR absorptions (cm^{-1}) of the ternary binuclear complexes

Comp. No.	$\nu(ClO_4)$ (cm^{-1})	ν(>C=N) (cm^{-1})	aromatic stretching ν(-C-H) (cm^{-1})	miscellaneous frequencies (cm^{-1})
3-I	1086	1613	3063	$\nu_{as}(-CH_2-)$ 2923
3-II	1108	1610	3064	$\nu_{as}(-O-)$ 1245
3-III	1087	1612	3084	$\nu_{as}(-CH_2-)$ 2920
3-IV	1090	1616	3080	$\nu_{as}(-O-)$ 1250
3-V	1103	1600	3062	$\nu_{as}(-CH_2-)$ 2922, $\nu(H_2O)$ 3500
3-VI	1091	1601	3060	$\nu_{as}(-O-)$ 1243, $\nu(H_2O)$ 3436
3-VII	1098	1600	3059	ν_{as} $(-SO_2-)$ 1338, $\nu_s(-SO_2-)$1144, $\nu(H_2O)$ 3438
3-VIII	1103	1600	3058	ν_{as} $(-SO_2-)$ 1336, $\nu_s(-SO_2-)$1140, $\nu(H_2O)$ 3436
3-IX	1098	1600	3055	$\nu_{as}(-CH_2-)$ 2924
3-X	1108	1603	3060	$\nu_{as}(-O-)$ 1243, $\nu(H_2O)$ 3438
3-XI	1101	1602	3061	ν_{as} $(-SO_2-)$ 1315, $\nu_s(-SO_2-)$ 1145, $\nu(H_2O)$ 3470
3-XII	1090	1610	3059	$\nu_{as}(-CH_2-)$ 2927, $\nu_{as}(C-O-CH_3)$ 1238, $\nu_s(C-O-CH_3)$ 1032
3-XIII	1108	1608	3060	$\nu_{as}(-O-)$ 1240, $\nu(H_2O)$ 3438, $\nu_s(C-O-CH_3)$ 1032
3-XIV	1098	1603	3056	ν_{as} $(-SO_2-)$ 1327, $\nu_s(-SO_2-)$1149, $\nu(H_2O)$ 3471, $\nu_{as}(C-O-CH_3)$1249, $\nu_s(C-O-CH_3)$ 1062
3-XV	1112	1604	3056	ν_{as} $(-SO_2-)$ 1327, $\nu_s(-SO_2-)$1149, $\nu(H_2O)$ 3538, $\nu_{as}(C-O-CH_3)$ 1249, $\nu_s(C-O-CH_3)$ 1062.

Continued .....

Comp. No.	$\nu(ClO_4)$ (cm^{-1})	$\nu(>C=N)$ (cm^{-1})	aromatic stretching $\nu(-C-H)$ (cm^{-1})	miscellaneous frequencies (cm^{-1})
3-XVII	1091	1608	3067	$\nu_{as}(-O-)$ 1240, $\nu_s(C-O-CH_3)$ 1032
3-XVIII	1107	1604	3070	ν_{as} ($-SO_2-$)1301, $\nu_s(-SO_2-)$1149, $\nu_{as}(C-O-CH_3)$ 1249, $\nu_s(C-O-CH_3)$1033
3-XIX	1095	1609	3081	ν_{as} ($-SO_2-$)1317, $\nu_s(-SO_2-)$1149, $\nu_{as}(C-O-CH_3)$ 1250, $\nu_s(C-O-CH_3)$ 1034

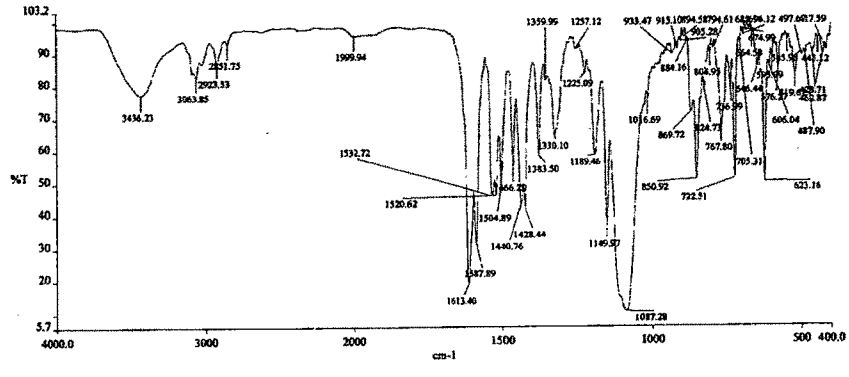

Fig. 3.2.1 FTIR spectrum of the binuclear complex, $[Cu_2(phen)_2salDPM](ClO_4)_2$.

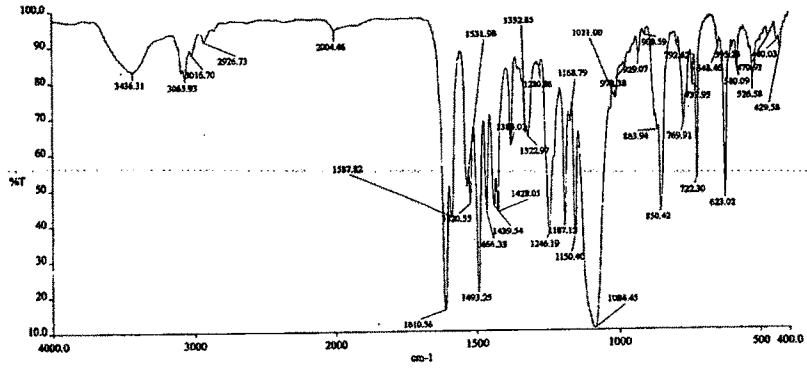

Fig.3.2.2 FTIR spectrum of the binuclear complex, $[Cu_2(phen)_2salDPE](ClO_4)_2$.

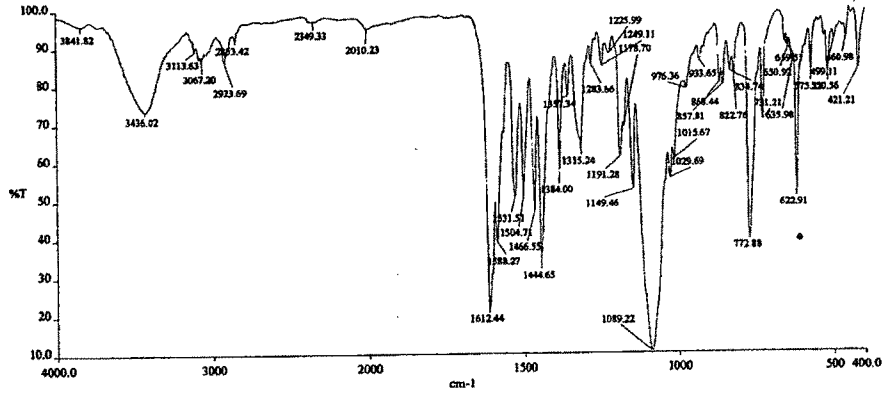

Fig.3.2.3 FTIR spectrum of the binuclear complex, $[Cu_2(bipy)_2salDPM](ClO_4)_2$

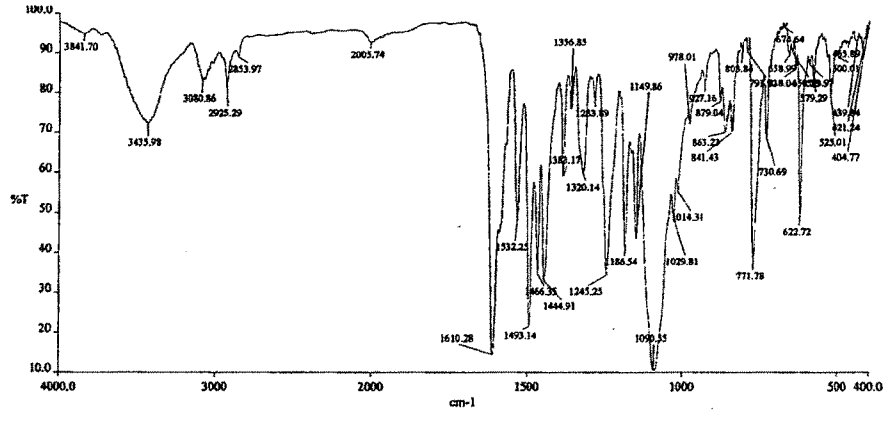

Fig. 3.2.4 FTIR spectrum of the binuclear complex, $[Cu_2(bipy)_2salDPE](ClO_4)_2$.

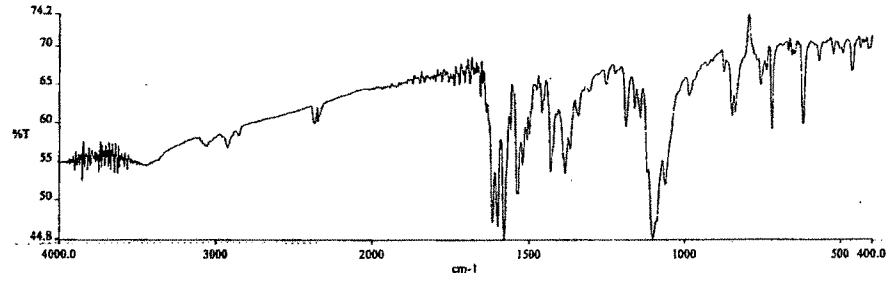

Fig.3.3.1 FTIR spectrum of the binuclear complex, $[Cu_2(phen)_2naphDPM](ClO_4)_2.2H_2O$.

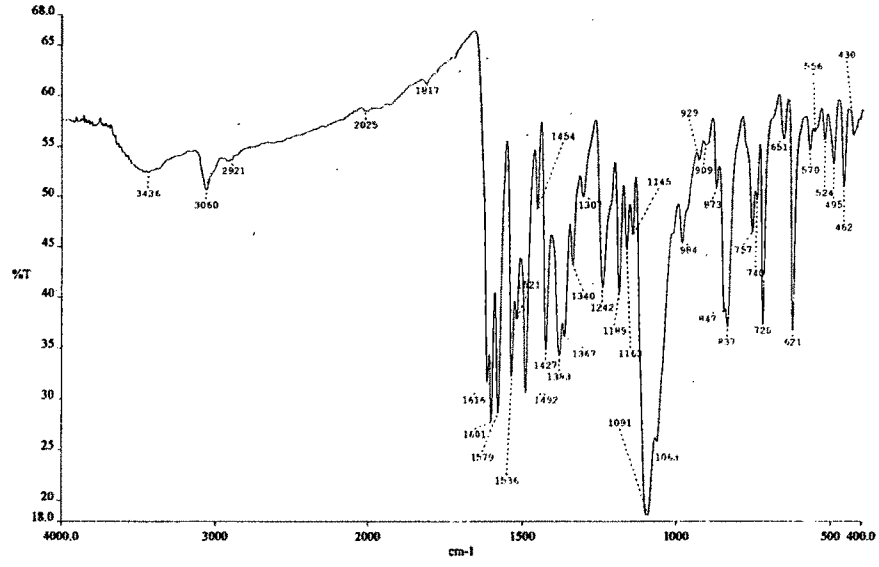

Fig. 3.3.2 FTIR spectrum of the binuclear complex, $[Cu_2(phen)_2naphDPE](ClO_4)_2.2H_2O$.

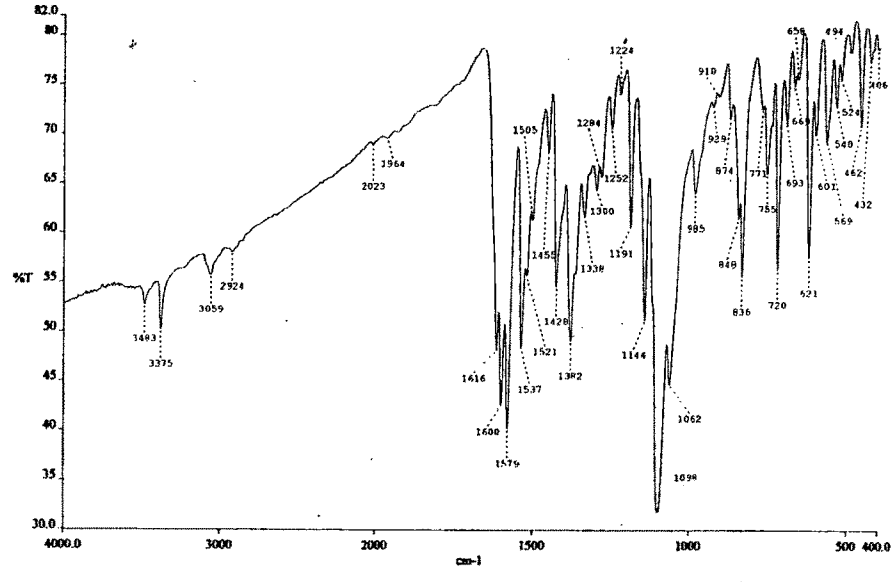

Fig.3.3.3 FTIR spectrum of the binuclear complex, $[Cu_2(phen)_2naph4\text{-}DPS](ClO_4)_2.2H_2O$.

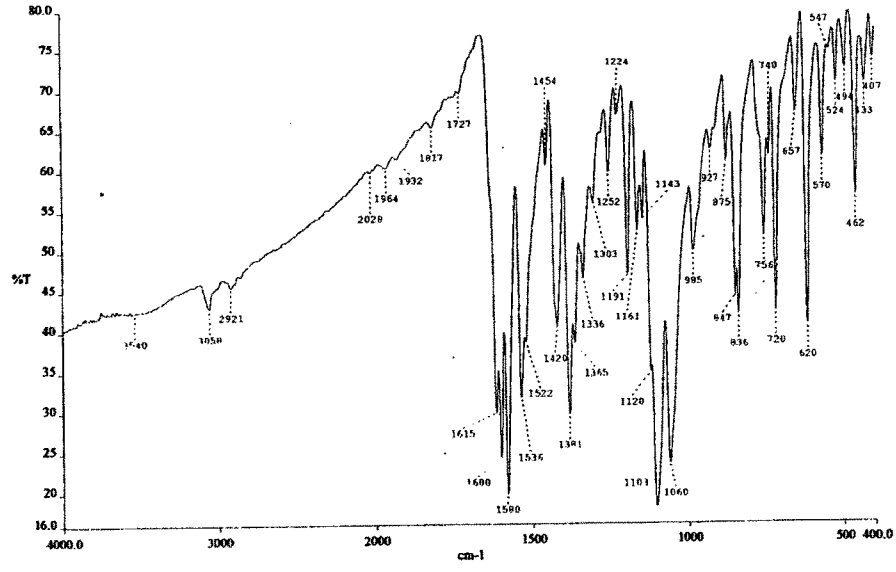

Fig. 3.3.4 FTIR spectrum of the binuclear complex, $[Cu_2(phen)_2naph3\text{-}DPS](ClO_4)_2.2H_2O$.

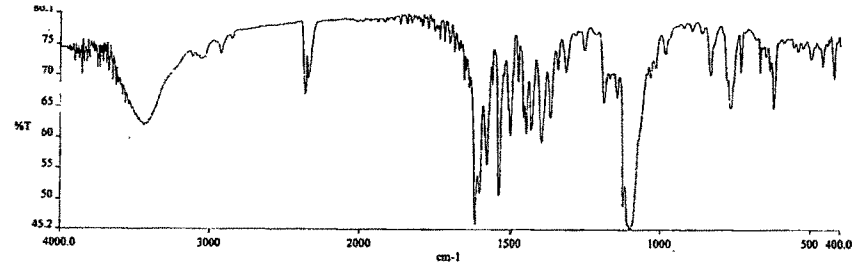

Fig.3.3.5 FTIR spectrum of the binuclear complex, $[Cu_2(bipy)_2naphDPM](ClO_4)_2$.

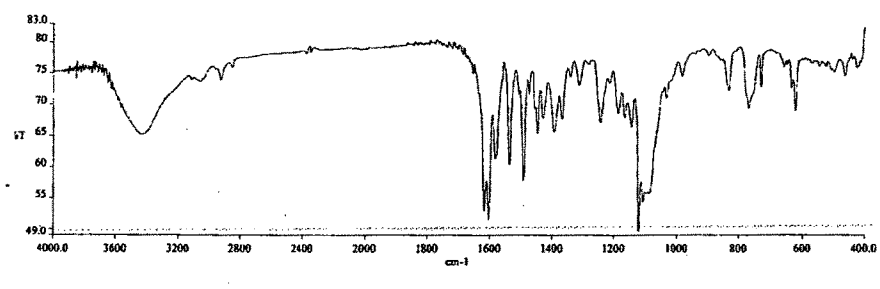

Fig.3.3.6 FTIR spectrum of the binuclear complex, $[Cu_2(bipy)_2naphDPE](ClO_4)_2.2H_2O$.

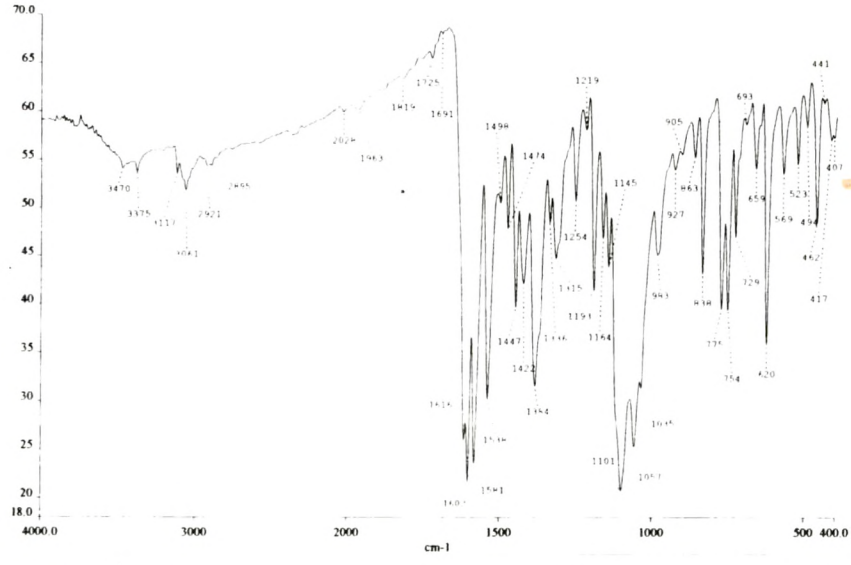

Fig.3.3.7 FTIR spectrum of the binuclear complex, $[Cu_2(bipy)_2naph3\text{-}DPS](ClO_4)_2.2H_2O$.

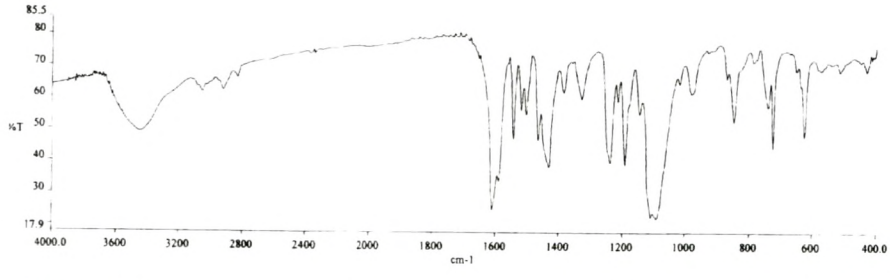

Fig.3.4.1 FTIR spectrum of the binuclear complex, $[Cu_2(phen)_2vanDPM](ClO_4)_2$.

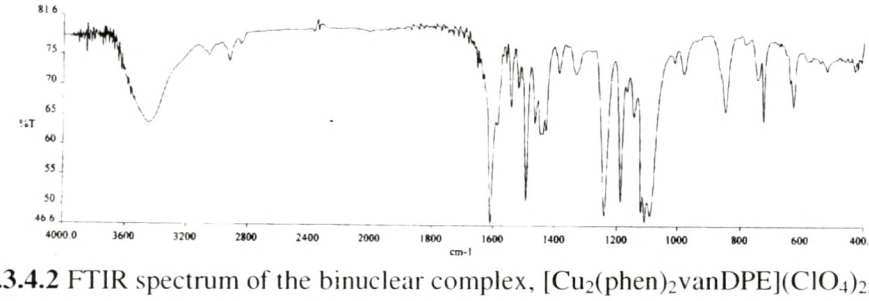

Fig.3.4.2 FTIR spectrum of the binuclear complex, $[Cu_2(phen)_2vanDPE](ClO_4)_2.2H_2O$

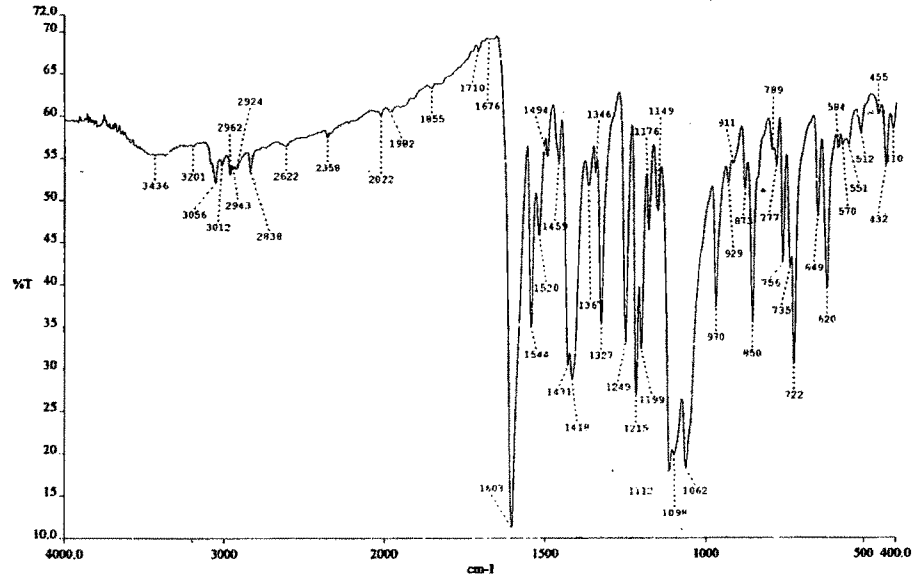

Fig.3.4.3 FTIR spectrum of the binuclear complex $[Cu_2(phen)_2van4\text{-}DPS](ClO_4)_2.2H_2O$.

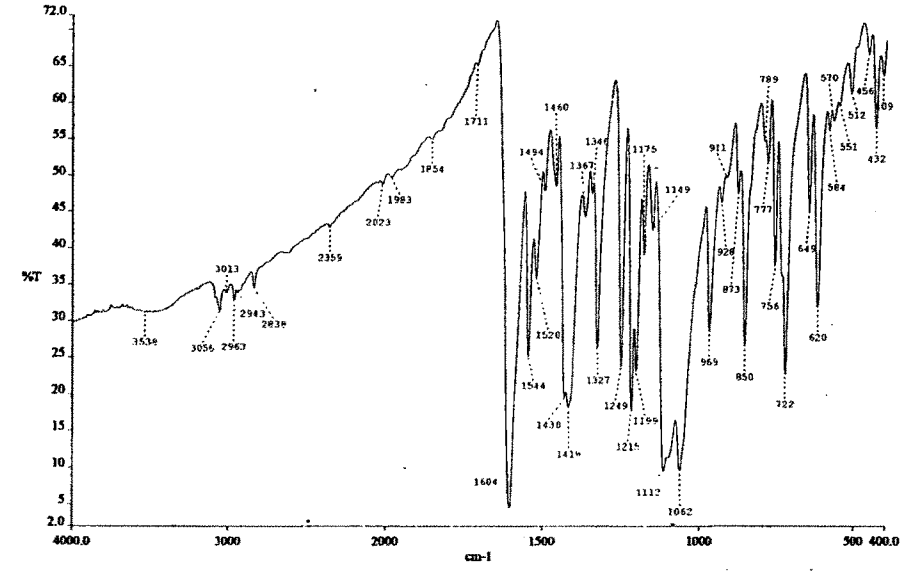

Fig.3.4.4 FTIR spectrum of the binuclear complex $[Cu_2(phen)_2van3\text{-}DPS](ClO_4)_2.2H_2O$.

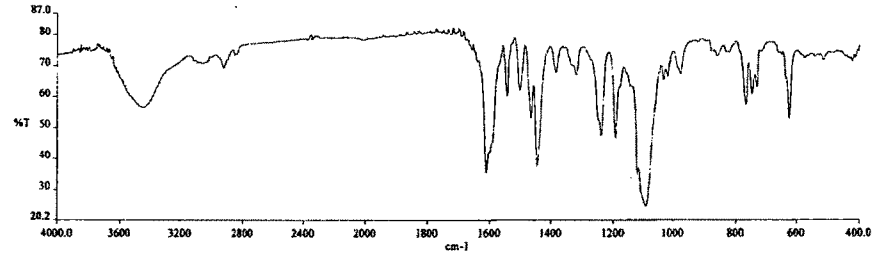

Fig.3.4.5 FTIR spectrum of the binuclear complex, $[Cu_2(bipy)_2vanDPM](ClO_4)_2$.

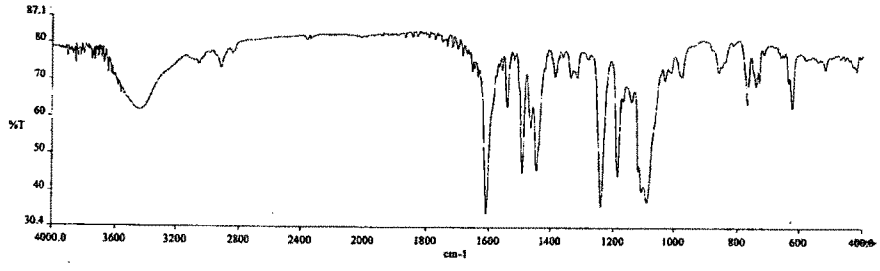

Fig.3.4.6 FTIR spectrum of the binuclear complex, $[Cu_2(bipy)_2vanDPE](ClO_4)_2$.

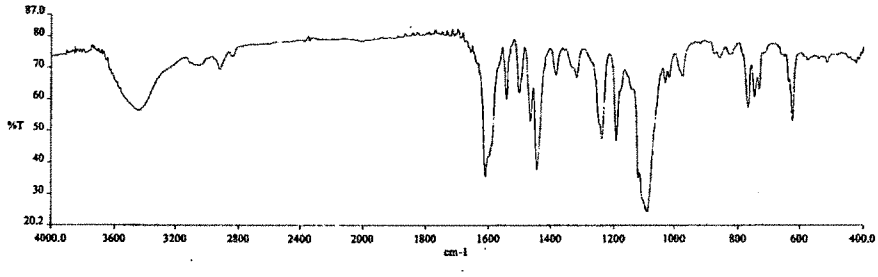

Fig.3.4.7 FTIR spectrum of the binuclear complex, $[Cu_2(bipy)_2van4\text{-}DPS](ClO_4)_2$.

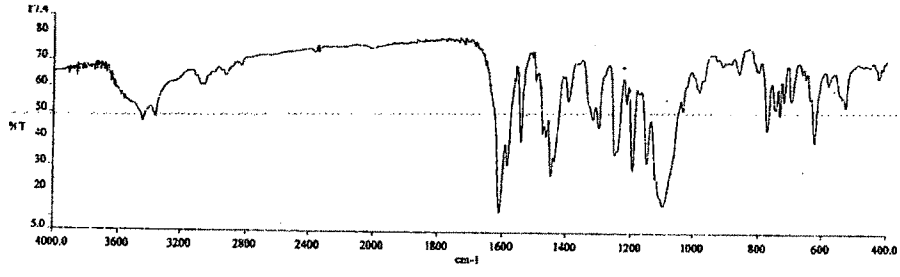

Fig.3.4.8 FTIR spectrum of the binuclear complex, $[Cu_2(bipy)_2van3\text{-}DPS](ClO_4)_2$.

3.3.3 Mass spectra:

FAB mass spectra of the complexes were recorded in m-nitrobenzyl alcohol as matrix. Though the solubility of the complexes in suitable solvents was poor, sufficiently informative spectra could be observed.

FAB mass spectrum of the complex $[Cu_2(bipy)_2salDPM](ClO_4)_2$ (**Fig. 3.5.1**) consists of parent binuclear monocation peak at m/z 846 with relative abundance value of 42%.

Complex, $[Cu_2(bipy)_2salDPM](ClO_4)_2$ lost the anions $2ClO_4^-$ to form the parent dication with m/z 422 which is observed with very low relative abundance. However, this species can add 4 H across the >C=N bonds. The resulting species is observed at m/z 846 with relative abundance 42%. Some important fragments with the observed m/z values are summarized in **Table 3.4.1** and the fragments formed are represented below.

Other important fragments include the dicopper species formed by loss of bipy (m/z 688), the species formed by loss of one Cubipy from the parent complex (m/z 624) and the free protonated binucleating ligand, $[H_3salDPM]^+$ (m/z 407). Also some mononuclear complex species like, $[Cubipy]^+$, $[Cu(bipy)_2]^+$ and $[CuLH]^+$ are observed. Smaller organic fragments formed by ligand dissociation have also been identified.

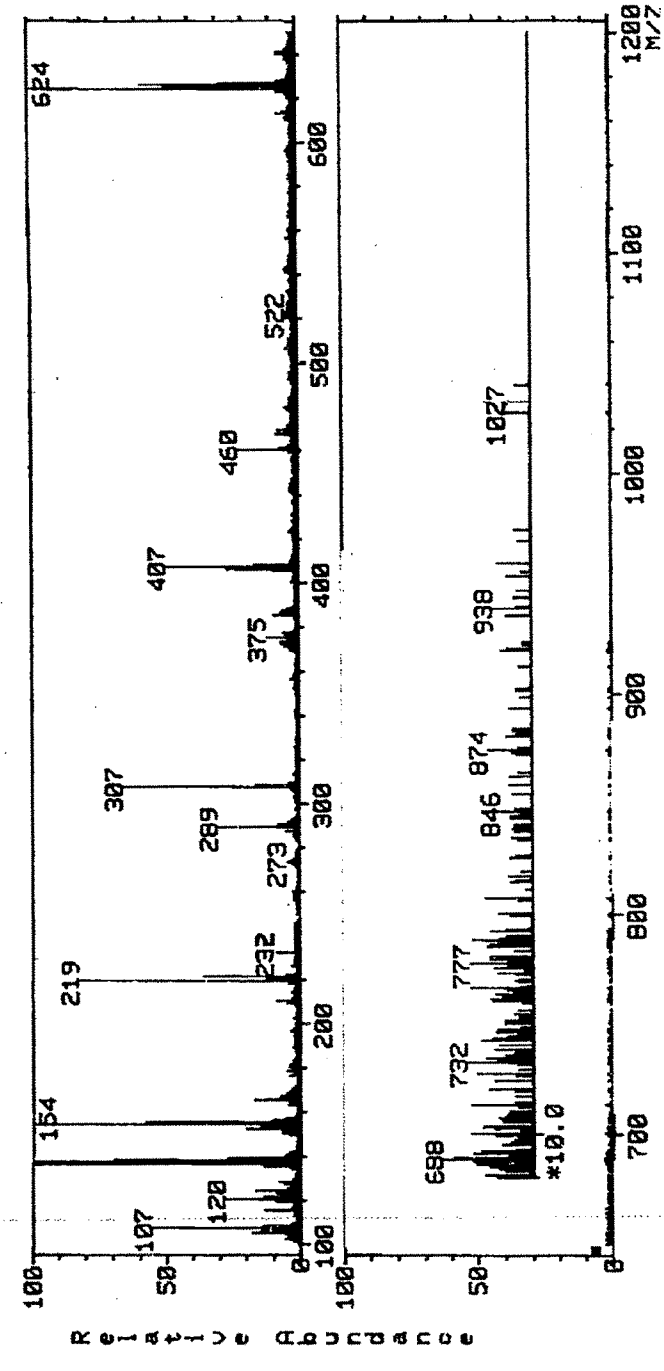

Fig. 3.5.1 FAB – Mass spectra of complex, $[Cu_2(bipy)_2salDPM](ClO_4)_2$

Table 3.4.1: Fragmentation pattern in the positive ion in FAB – MS of $[Cu_2(bipy)_2salDPM](ClO_4)_2$ in m-nitrobenzyl alcohol.

m/z (% relative abundance)	**Molecular formula of the fragment**
846 (42%)	$[C_{47}H_{40}N_6O_2Cu_2]^+$ (parent ion peak)
688 (63%)	$[C_{37}H_{30}N_4O_2Cu_2]^+$
624 (100%)	$[C_{37}H_{29}N_4O_2Cu]^+$
470 (8%)	$[C_{27}H_{23}N_2O_2Cu]^+$
407 (48%)	$[C_{27}H_{23}N_2O_2]^+$ (SB-ligand)
375 (12%)	$[C_{20}H_{16}N_4Cu]^+$, $[Cu(bipy)_2]$
219 (60%)	$[C_{10}H_8N_2Cu]^+$,Cu(bipy)]
120 (28%)	$[C_7H_6NO]^+$ OR $[C_8H_{10}N]^+$
107 (58%)	$[C_7H_7O]^+$ OR $[C_7H_9N]^+$

Possible structure of $[Cu_2(bipy)_2salDPM]^{2+}$ and the corresponding fragments in FAB-Mass:

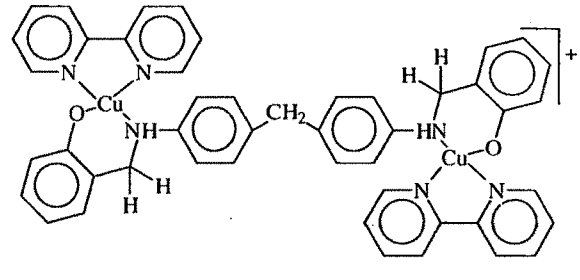

m/z 846 (42%), $[C_{47}H_{40}N_6O_2Cu_2]^+$

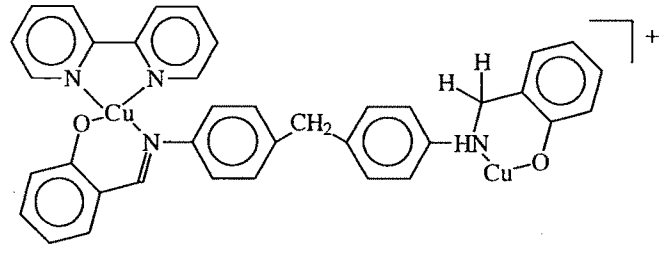

m/z 688 (63%), $[C_{37}H_{30}N_4O_2Cu_2]^+$

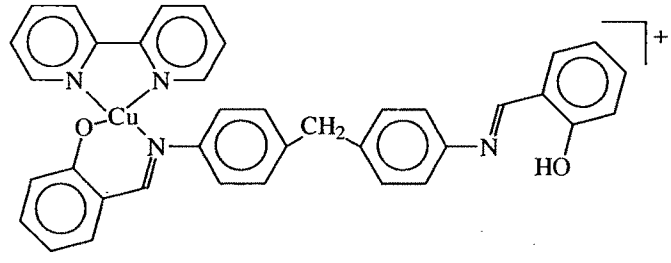

m/z 624 (100%), $[C_{37}H_{29}N_4O_2Cu]^+$

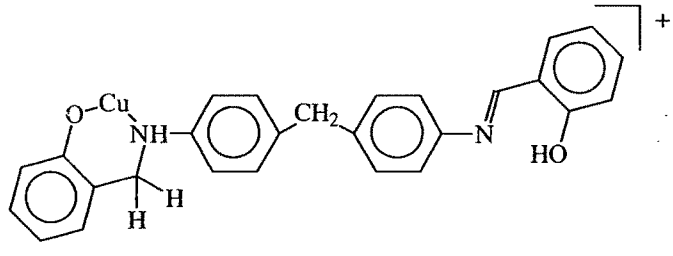

m/z 470 (8%), $[C_{27}H_{23}N_2O_2Cu]^+$

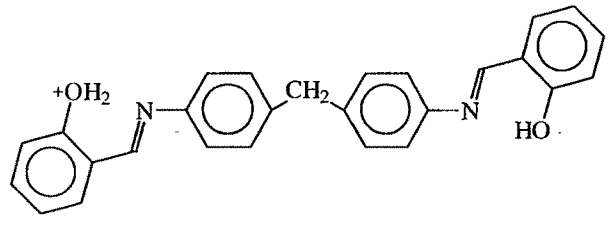

m/z 407, $[C_{27}H_{23}N_2O_2]^+$ (SB-ligand)

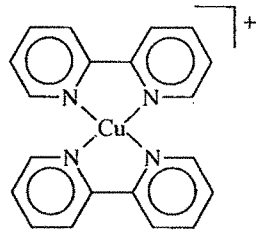

m/z 375 (12%), $[C_{20}H_{16}N_4Cu]^+$

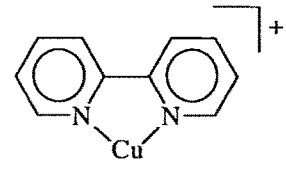

m/z 219 (60%), $[C_{10}H_8N_2Cu]^+$

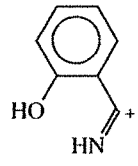

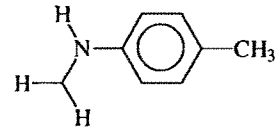

m/z 120 (28%), $[C_8H_{10}N]^+$ OR $[C_7H_6NO]^+$

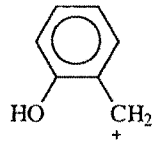

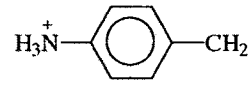

m/z 107 (58%), $[C_7H_7O]^+$ OR $[C_7H_9N]^+$

FAB mass spectrum of the complex $[Cu_2(bipy)_2naphDPM](ClO_4)_2$ consists of parent binuclear monocation peak at m/z 789 with relative abundance value of 36%.

A peak corresponding to the parent dication, $[Cu_2(bipy)_2naphDPM]^{2+}$, is observed at m/z = 571 in the FAB-Mass spectrum of the complex. A mononuclear complex $[CubipyLH]^+$, (m/z = 724) formed after the loss of one [Cubipy] from the parent dication, the free protonated binucleating ligand m/z = 507 and $[Cubipy]^+$ (m/z = 219) are among the other important species observed, (**Fig.3.5.2, Table-3.4.2**).

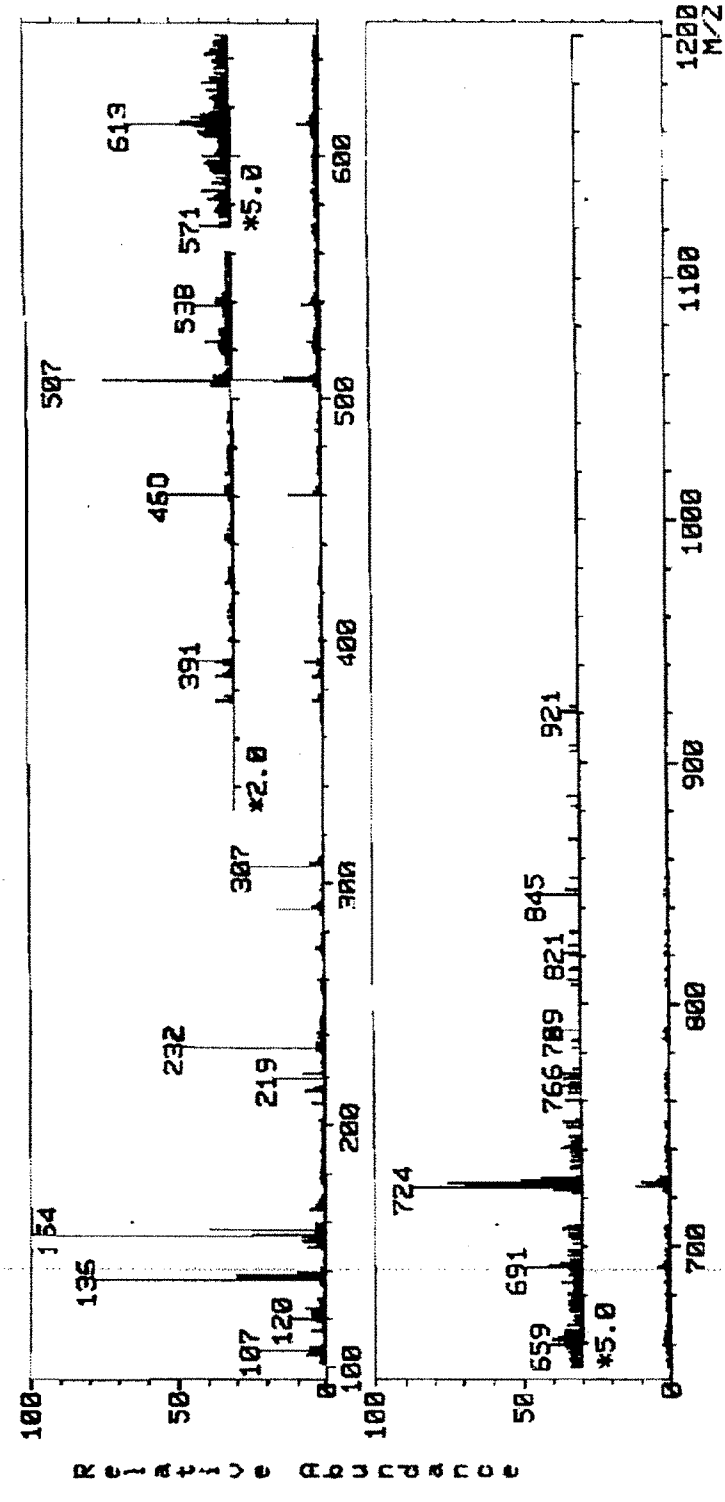

Fig. 3.5.2 FAB – Mass spectra of the complex, $[Cu_2(bipy)_2naphDPM](ClO_4)_2$

Table 3.4.2: Fragmentation pattern in the positive ion in FAB–MS of $[Cu_2(bipy)_2naphDPM](ClO_4)_2$ in m-nitrobenzyl alcohol.

m/z (% relative abundance)	**Molecular formula of the fragment**
724 (84%)	$[C_{45}H_{33}N_4O_2Cu]^+$
	[CubipyLH]$^+$
789 (36%)	$[C_{45}H_{35}N_4O_2Cu_2]^+$
571 (28%)	$[C_{55}H_{41}N_6O_{10}Cl_2Cu_2]^{2+}$
571 (28%)	$[C_{35}H_{28}N_2O_2Cu]^+$
507 (84%)	$[C_{35}H_{27}N_2O_2]^+$ (SB)
391 (56%)	$[C_{21}H_{18}N_3OCu]^+$
232 (48%)	$[C_{11}H_7NOCu]^+$
219 (16%)	$[C_{10}H_8Cu]^+$
120 (6%),	$[C_7H_6NO]^+$
107 (11%),	$[C_7H_7O]^+$

Possible structure of $[Cu_2(bipy)_2naphDPM]^{2+}$ and the corresponding fragments in FAB-Mass:

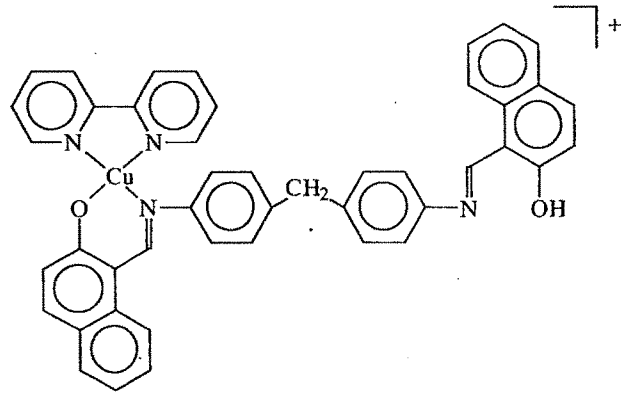

m/z 724 (84%), $[C_{45}H_{33}N_4O_2Cu]^+$, [CubipyLH]$^+$

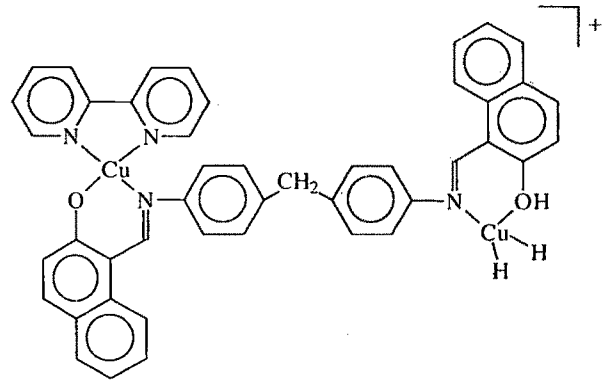

m/z 789 (36%), $[C_{45}H_{35}N_4O_2Cu_2]^+$

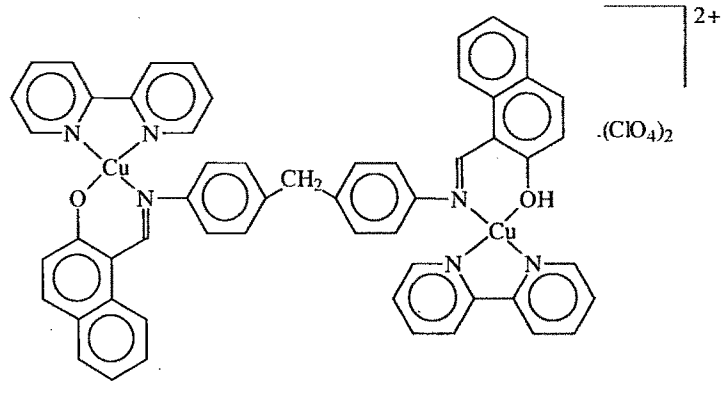

m/z 571 (28%), $[C_{55}H_{41}N_6O_{10}Cl_2Cu_2]^{2+}$

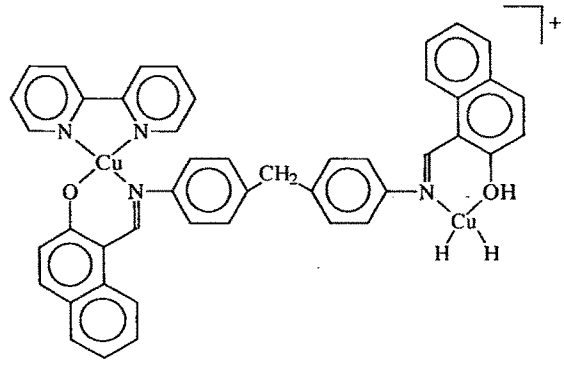

m/z 571 (28%), $[C_{35}H_{28}N_2O_2Cu]^+$

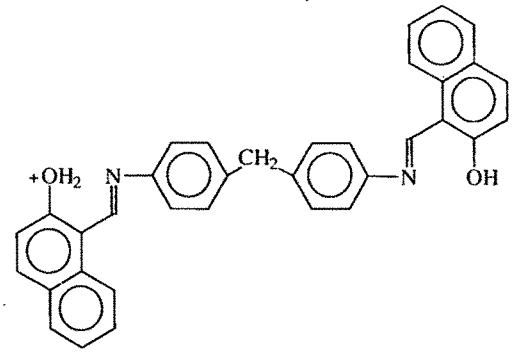

m/z 507 (84%), $[C_{35}H_{27}N_2O_2]^+$, (SB-ligand)

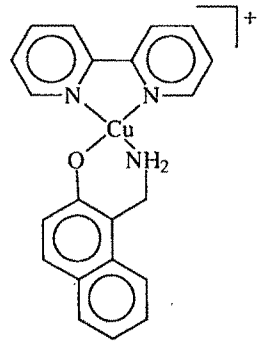

m/z 391 (56%) $[C_{21}H_{18}N_3OCu]^+$,

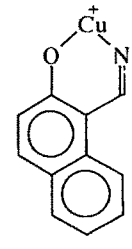

m/z 232 (48%), $[C_{11}H_7NOCu]^+$

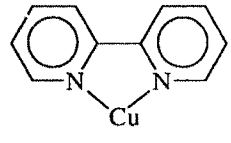

m/z 219 (16%), $[C_{10}H_8N_2Cu]^+$

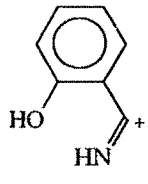

120 (6%), $[C_7H_6NO]^+$

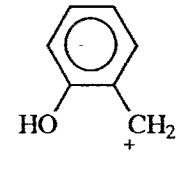

107 (11%), $[C_7H_7O]^+$

In the FAB mass spectrum of the complex $[Cu_2(bipy)_2van3\text{-}DPS](ClO_4)_2$, the parent ion peak can be observed at m/z = 1151. This is formed by protonation of the complex molecule, $[M+H^+]$. The dication corresponding to $[M+2H^+]$ is observed at m/z = 578. The complex cation on association with one H forms the species with m/z = 953 (6%), (**Fig.3.5.3, Table 3.4.3**).

All these peaks assigned in the above three complexes strongly supported the formation of binuclear complexes with suggested molecular formulae.

The peaks corresponding to the fragments of m-nitrobenzyl alcohol and associated products are observed at m/z 136, 137, 154, 289 and 307. These fragments get associated with various fragments formed by the metal complexes and thus give rise to a number of species with low abundance and are responsible for the minor peaks.

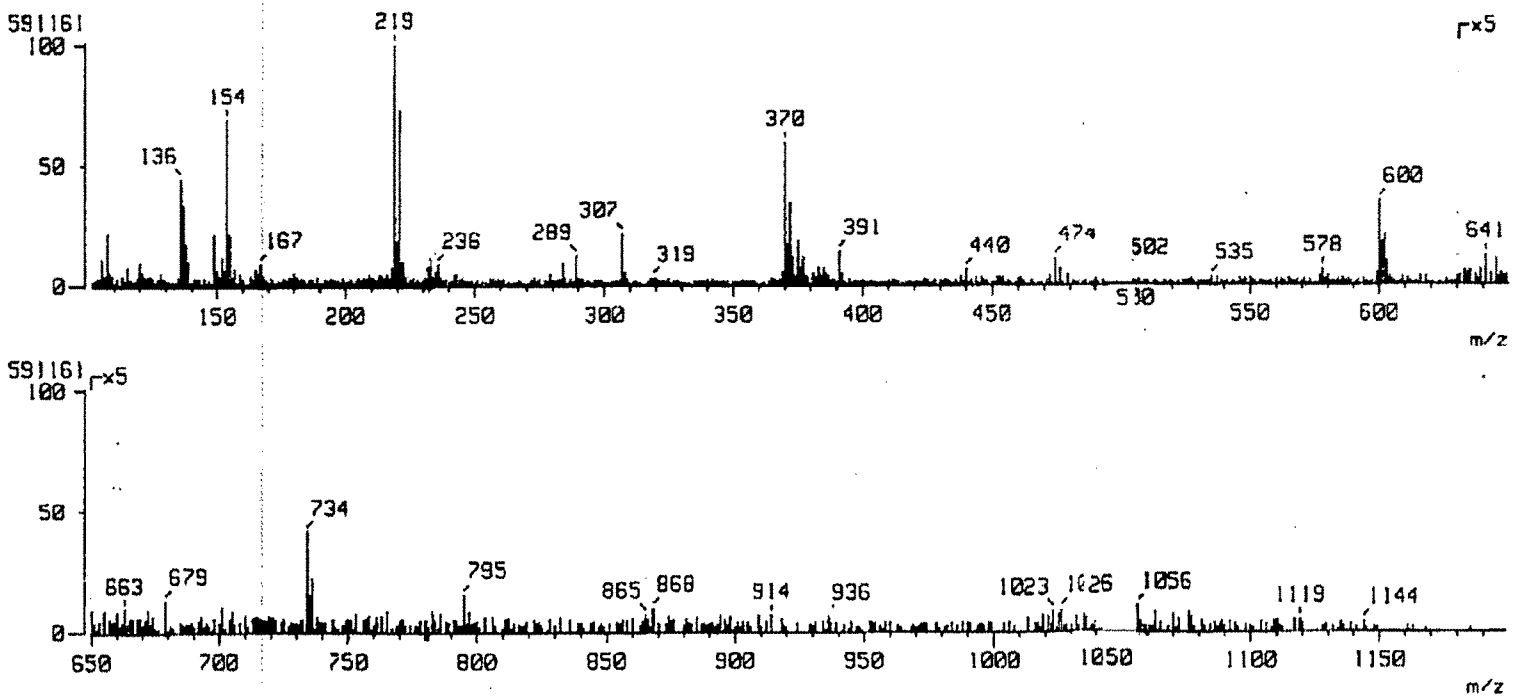

Fig.3.5.3 FAB - Mass spectra of complex, $[Cu_2(bipy)_2van3\text{-}DPS](ClO_4)_2$.

Table 3.4.3: Fragmentation pattern in the positive ion in FAB–MS of $[Cu_2(bipy)_2van3\text{-}DPS](ClO_4)_2$ in m-nitrobenzyl alcohol.

m/z (% relative abundance)	**Molecular formula of the fragment**
476(8%)	$[C_{48}H_{38}N_6O_6SCu_2]^{2+}$
474 (17%)	$[C_{48}H_{34}N_6O_6SCu_2]^{2+}$ (binuclear dication)
953 (6%)	$[C_{48}H_{39}N_6O_6SCu_2]^{+}$ (parent ion peak)
795 (17%)	$[C_{38}H_{30}N_4O_6SCu_2\ ]^{+}\text{-}H]^{+}$
736 (24%)	$[C_{38}H_{33}N_4O_6SCu]^{+}$
734 (43%)	$[C_{38}H_{31}N_4O_6SCu]^{+}$
578 (7%)	$[C_{48}H_{44}N_6O_{14}Cl_2SCu_2]^{2+}$
578 (7%)	$[C_{28}H_{23}N_2O_6SCu]^{+}$, (Cu-SB)
375 (19%)	$[C_{20}H_{16}N_4Cu]^{+}$
370 (61%)	$[C_{18}H_{17}N_3O_2Cu]^{+}$ (mononuclear complex)
219 (100%)	$[C_{10}H_8N_2Cu]^{+}$
167 (10%)	$[C_7H_5O_2S\ N]^{+}$
149 (22%)	$[C_8H_7NO_2]^{+}$

Possible structure of $[Cu_2(bipy)_2van3\text{-}DPS]^{2+}$ and the corresponding fragments in FAB-Mass:

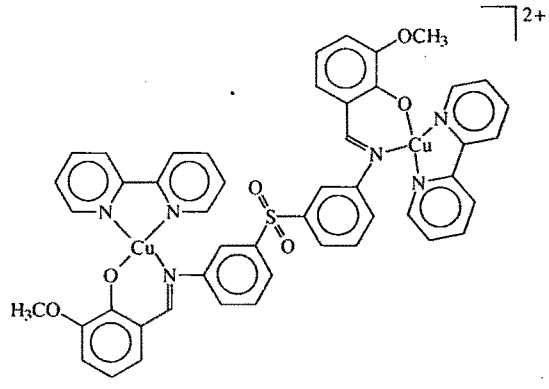

m/z 476 (8%), $[C_{48}H_{38}N_6O_6SCu_2]^{2+}$

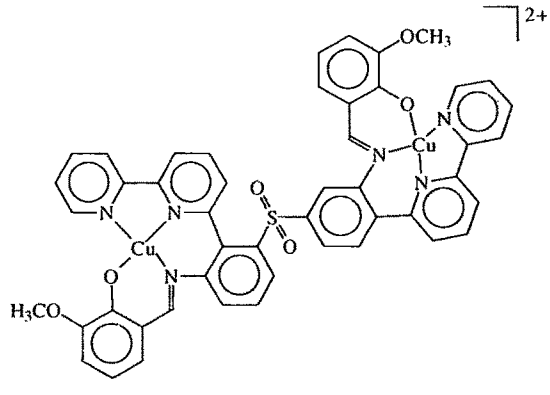

m/z 474 (17%), $[C_{48}H_{34}N_6O_6SCu_2]^{2+}$

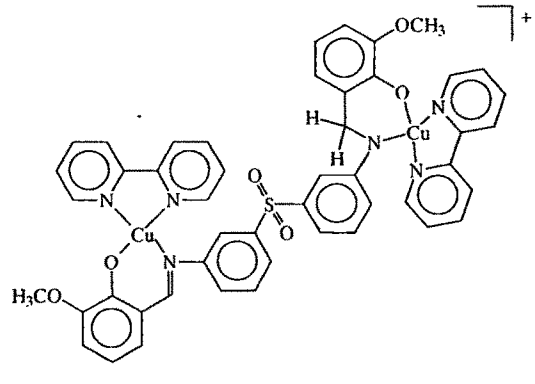

m/z 953 (6%), $[C_{48}H_{39}N_6O_6SCu_2]^{+}$

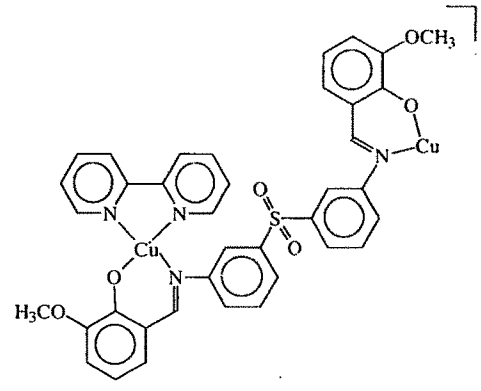

m/z 795 (17%), $[C_{38}H_{30}N_4O_6SCu_2]^+ - H]^+$

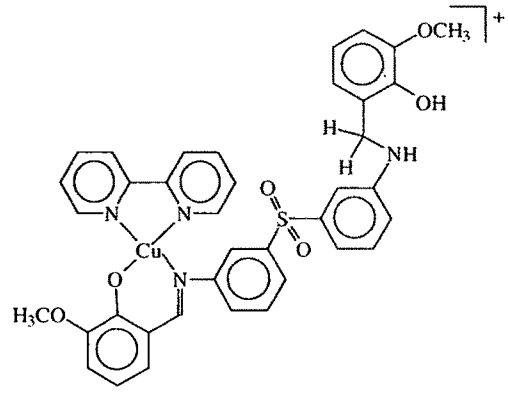

m/z 736 (24%), $[C_{38}H_{33}N_4O_6SCu]^+$

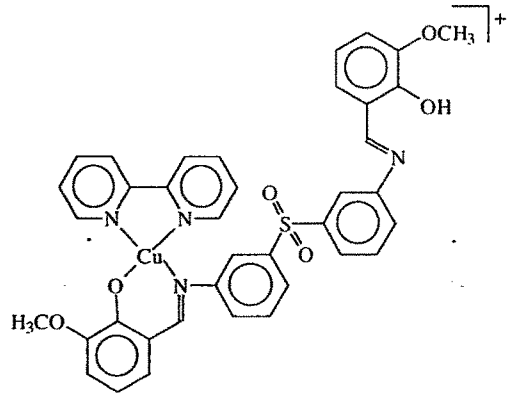

m/z 734 (43%), $[C_{38}H_{31}N_4O_6SCu]^+$

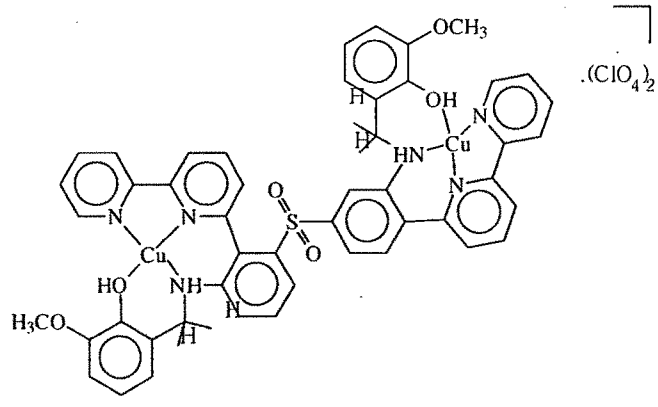

m/z 578 (7%), $[C_{48}H_{44}N_6O_{14}Cl_2SCu_2]^{2+}$

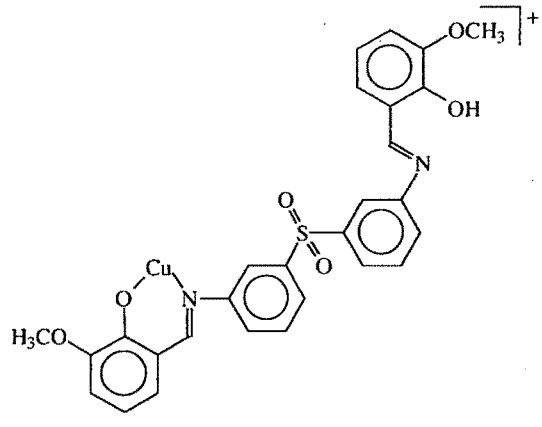

m/z 578 (7%), $[C_{28}H_{23}N_2O_6SCu]^+$

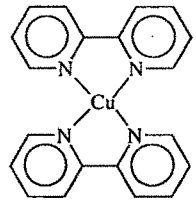

m/z 375 (19%), $[C_{20}H_{16}N_4Cu]^+$

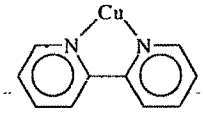

m/z 219 (100%), $[C_{10}H_8N_2Cu]^+$

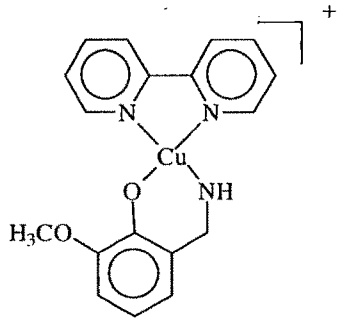

m/z 370 (61%), $[C_{18}H_{17}N_3O_2Cu]^+$

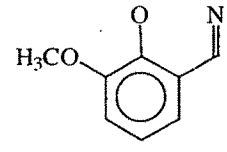

m/z 149 (22%), $[C_8H_7NO_2]^+$

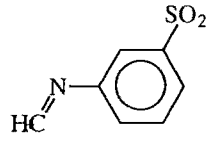

m/z 167 (10%), $[C_7H_5O_2S\,N]^+$

3.3.4 ESR spectral studies:

The ESR spectra of polycrystalline complexes, **3-I, 3-II, 3-III** and **3-IV** were recorded at room temperature while those of complexes **3-IX, 3-XVIII** and **3-XIX** were recorded in the form of DMSO glass at liq. N_2 temperature. The spectra are given in **Fig. 3.6.1** to **Fig. 3.6.11**, and results are summarized in **Table 3.5.1 and Table 3.5.2.** The ESR spectra of complexes **3-IX** and **3-XII** were recorded at RT and LNT are identical while the ESR of **3-XVIII** and **3-XIX** recorded at LNT shows clear hyperfine coupling with copper nuclear spin (I = 3/2).

Table 3.5.1 ESR parameters of ternary binuclear complexes at Room Temperature.

Comp No.	Complexes	Room Temperature	
3-I	$[Cu_2(phen)_2salDPM](ClO_4)_2$	$g_{\parallel}$, 2.21946	$g_{\perp}$, 2.06878
3-II	$[Cu_2(phen)_2salDPE](ClO_4)_2$	$g_{\parallel}$, 2.20738	$g_{\perp}$, 2.06774
3-III	$[Cu_2(bipy)_2salDPM](ClO_4)_2$	$g_{\parallel}$, 2.22601	$g_{\perp}$, 2.06754
3-IV	$[Cu_2(bipy)_2salDPE](ClO_4)_2$	$g_{\parallel}$, 2.21484	$g_{\perp}$, 2.06922

Table 3.5.2 ESR parameters of ternary binuclear complexes at RT and LNT.

Comp. No	Complexes	Room Temperature	LNT in DMSO
3-IX	$[Cu_2(bipy)_2naphDPM](ClO_4)_2$	$g_{\parallel}$, 2.13849	$g_{\parallel}$, 2.14915
		$g_{\perp}$, 2.05363	$g_{\perp}$, 2.06017
3-XII	$[Cu_2(bipy)_2vanDPM](ClO_4)_2$	$g_{\parallel}$, 2.16352	$g_{\parallel}$, 2.16352
		$g_{\perp}$, 2.08004	$g_{\perp}$, 2.08004
3-XVIII	$[Cu_2(bipy)_2van4\text{-}DPS](ClO_4)_2$	g_x, 2.06336	g_x, 1.91981
		g_y, 2.16299	g_y, 2.02464
		g_z, 2.22606	$A_y(G)$, 3.7809×10^{-3} cm^{-1}
			g_z, 2.31336
			$A_z(G)$, 1.728×10^{-2} cm^{-1}
3-XIX	$[Cu_2(bipy)_2van3\text{-}DPS](ClO_4)_2$	g_x, 2.26096	g_x, 1.91981
		g_y, 2.11367	g_y, 2.03097
		g_z, 2.05023	$A_y(G)$, 2.845×10^{-3} cm^{-1}
			g_z, 2.24532
			$A_z(G)$, 1.834×10^{-2} cm^{-1}

All complexes except $[Cu_2(bipy)_2van4\text{-}DPS](ClO_4)_2$ and $[Cu_2(bipy)_2van3\text{-}DPS](ClO_4)_2$ have typical axial ESR with well separated $g_{\parallel}$ and $g_{\perp}$ components. Complexes $[Cu_2(bipy)_2van4\text{-}DPS](ClO_4)_2$ and $[Cu_2(bipy)_2van3\text{-}DPS](ClO_4)_2$ have typical rhombic ESR with well resolved g_x, g_y and g_z components.

The observed $g_{\parallel}$ and $g_{\perp}$ values are within the range of values expected and reported in the literature [20, 21] for Cu^{2+} in near square planar or compressed tetrahedral geometry. The values of hyperfine coupling constant are, however, much lower indicating substantial delocalization of Cu^{2+} electron density over the ligand due to significant M→C π-interaction.

The complexes $[Cu_2(bipy)_2van4\text{-}DPS](ClO_4)_2$ and $[Cu_2(bipy)_2van3\text{-}DPS](ClO_4)_2$ exhibit a transition at half field. This is the forbidden $\Delta Ms=2$ transition, becoming partially allowed. The appearance of this transition confirms the existence of triplet state and spin coupling in the complexes.

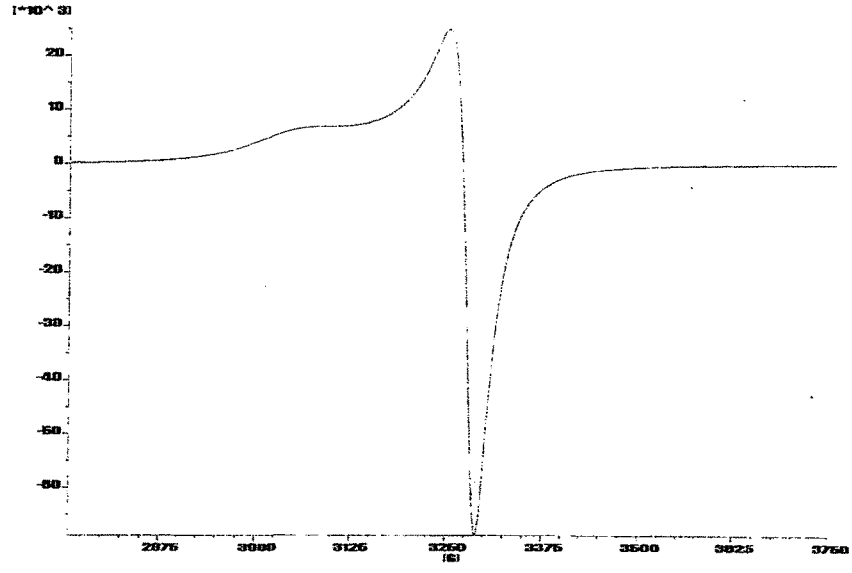

Fig.3.6.1 ESR of the binuclear complex, $[Cu_2(phen)_2salDPM](ClO_4)_2$ at RT.

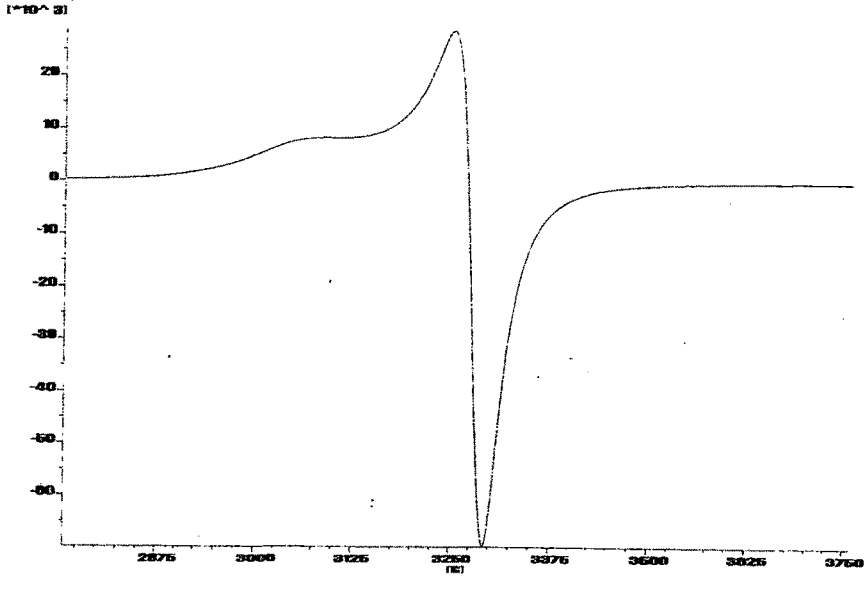

Fig.3.6.2 ESR of the binuclear complex, $[Cu_2(phen)_2salDPE](ClO_4)_2$ at RT.

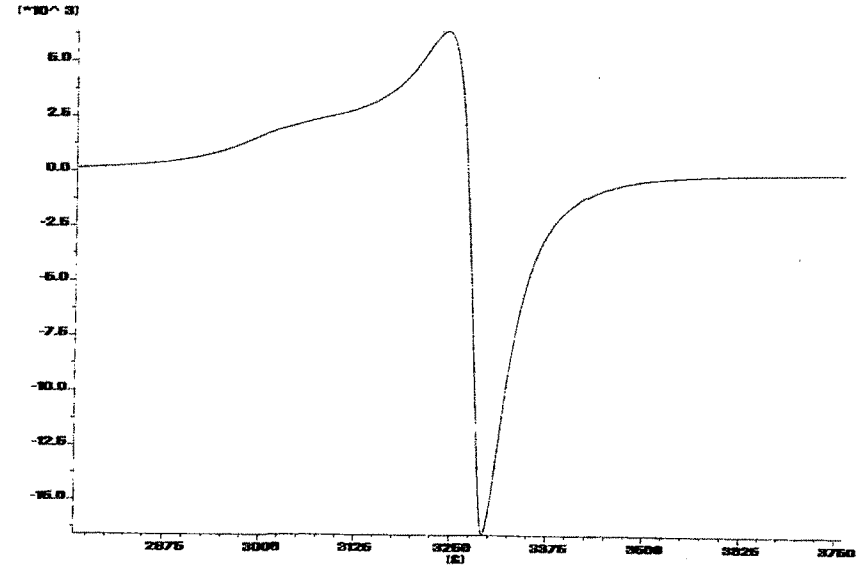

Fig.3.6.3 ESR of the binuclear complex, $[Cu_2(bipy)_2salDPM](ClO_4)_2$ at RT.

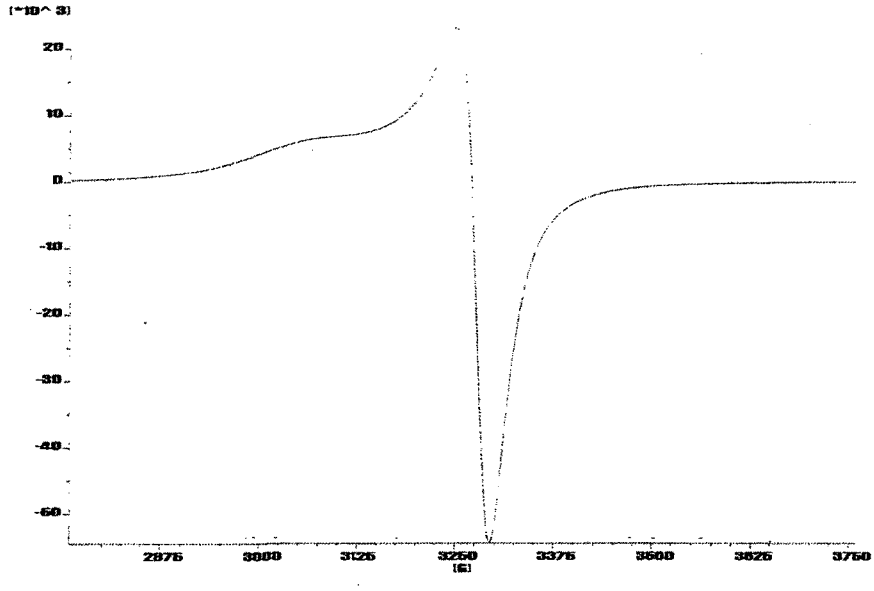

Fig.3.6.4 ESR of the binuclear complex, $[Cu_2(bipy)_2salDPE](ClO_4)_2$ at RT.

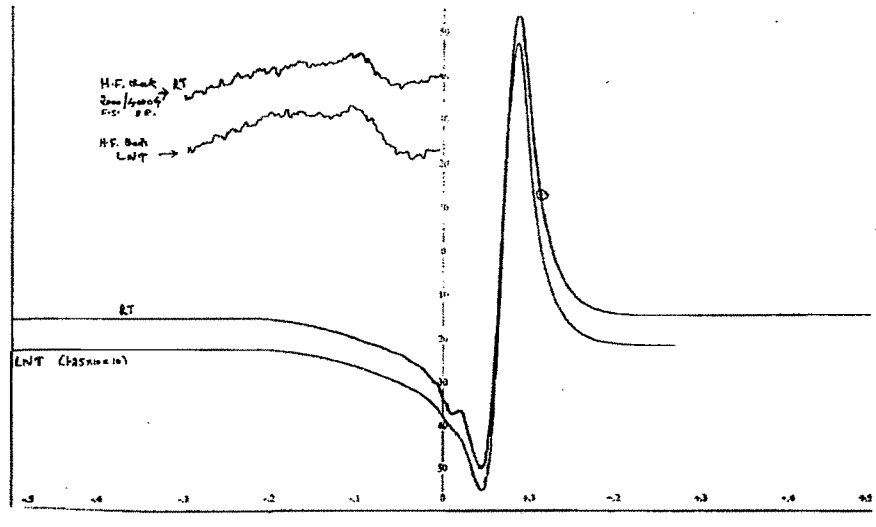

Fig.3.6.5 ESR of the binuclear complex, $[Cu_2(bipy)_2naphDPM](ClO_4)_2$ at RT and LNT.

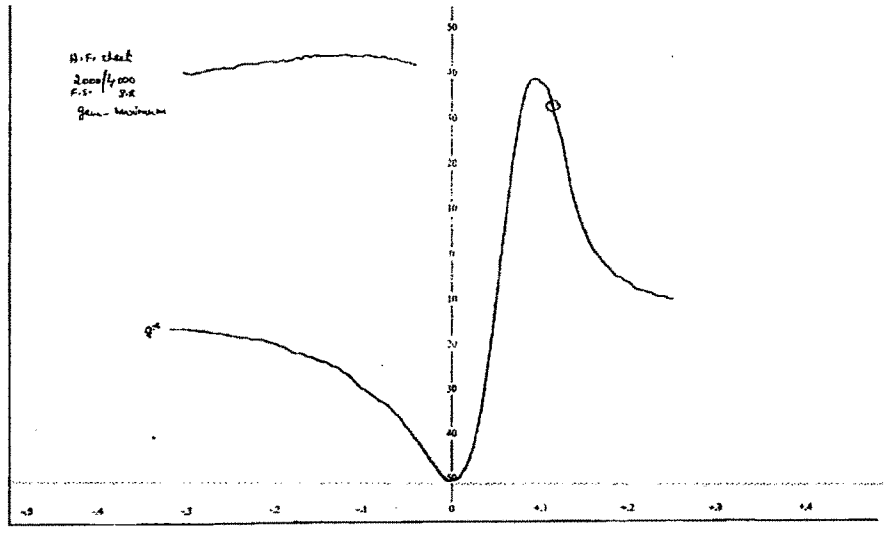

Fig. 3.6.6 ESR of the binuclear complex, $[Cu_2(bipy)_2vanDPM](ClO_4)_2$ at RT.

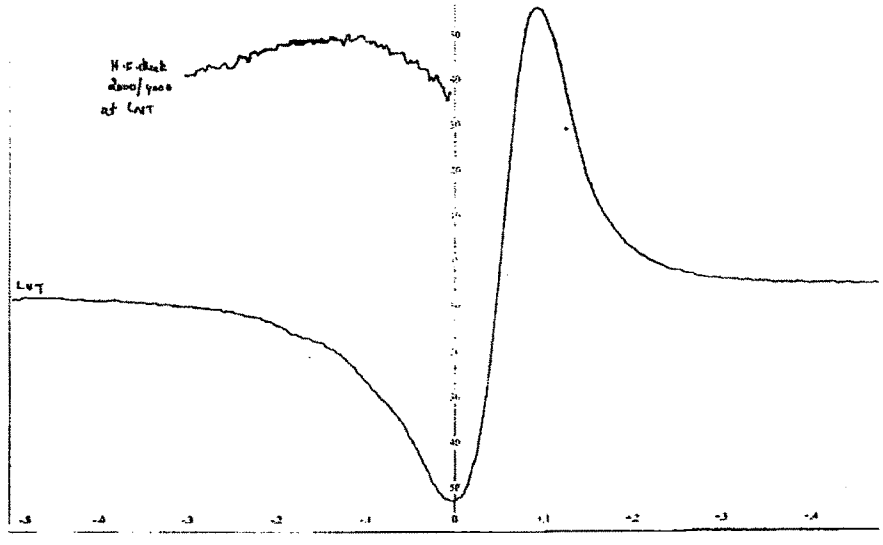

Fig. 3.6.7 ESR of the binuclear complex, $[Cu_2(bipy)_2vanDPM](ClO_4)_2$ at LNT.

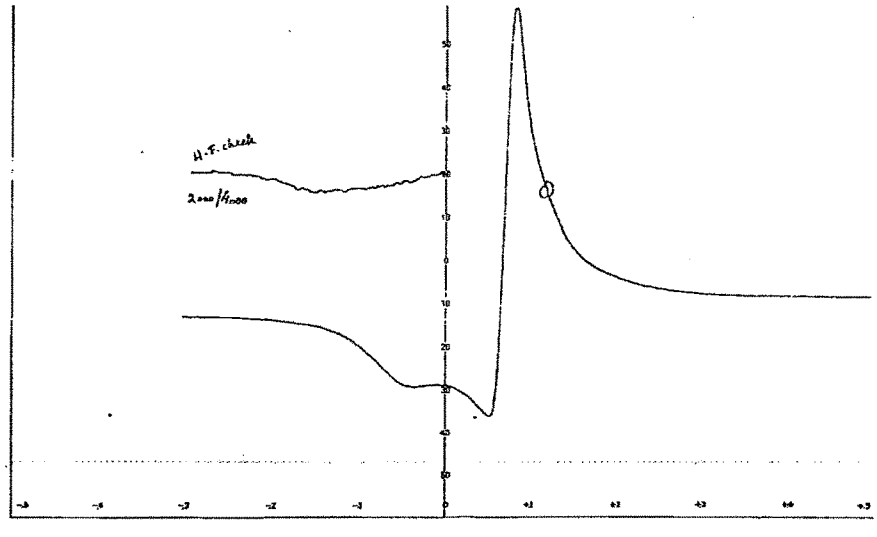

Fig.3.6.8 ESR of the binuclear complex, $[Cu_2(bipy)_2van4\text{-}DPS](ClO_4)_2$ at RT.

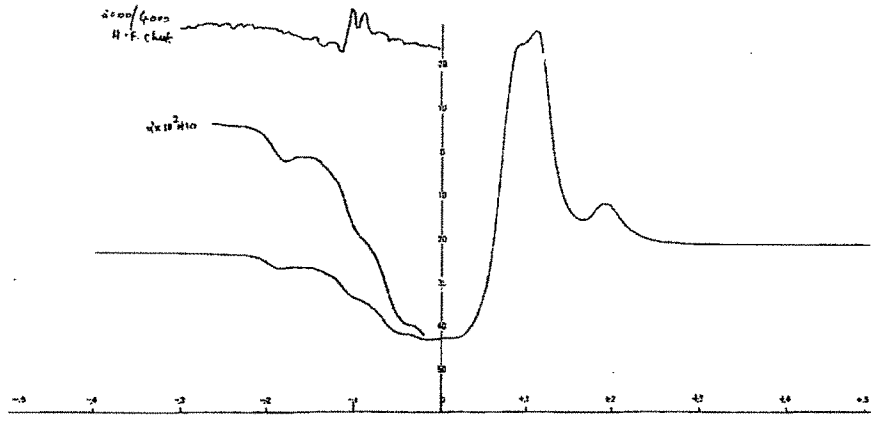

Fig.3.6.9 ESR of the binuclear complex, $[Cu_2(bipy)_2van4\text{-}DPS](ClO_4)_2$ at LNT.

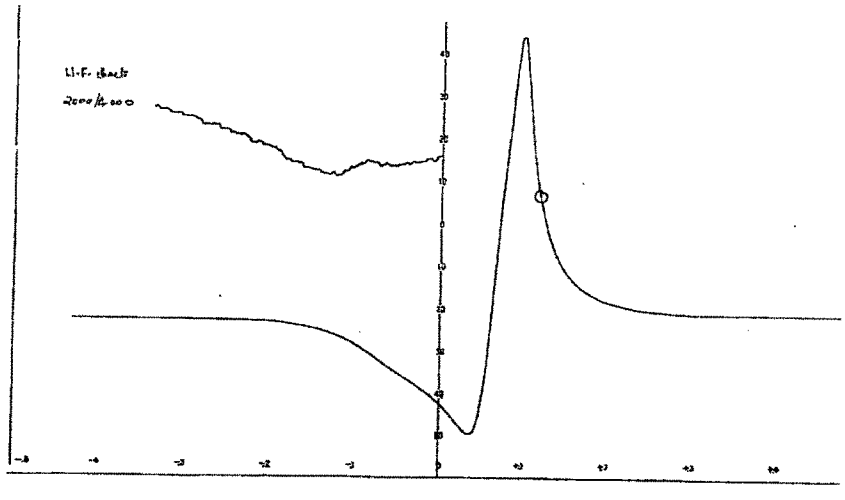

Fig.3.6.10 ESR of the binuclear complex, $[Cu_2(bipy)_2van3\text{-}DPS](ClO_4)_2$ at RT.

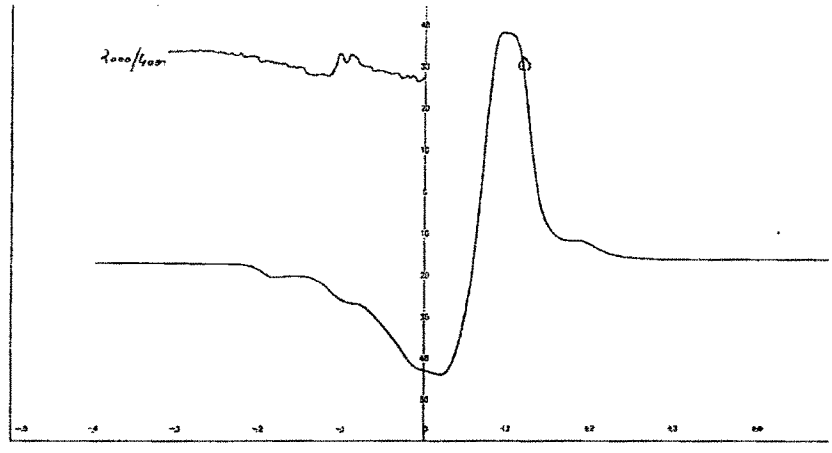

Fig. 3.6.11 ESR of the binuclear complex, $[Cu_2(bipy)_2van3\text{-}DPS](ClO_4)_2$ at LNT.

3.3.5 Magnetic properties:

The complexes studied here have a single bridging group and the other non-bridging positions around the metal ion occupied by π-bonding ligands. The single bridging group can allow a lot of flexibility in the structure while the π-bonding ligands and the functional groups over the bridging ligand can modulate the strength of M-L binding and the coordination geometry. Thus a lot of variation is expected in the geometrical parameters which can affect the spin exchange interaction.

The least square fit of the magnetic susceptibility data to Bleaney – Bower's equation in complexes, **3-III, 3-IV, 3-V, 3-VI, 3-VII, 3-VIII, 3-IX, 3-X, 3-XI, 3-XII, 3-XVI, 3-XVII, 3-XVIII** and **3-XIX,** yield J values ranging between -9.0 to 70 cm^{-1} i.e. the type of magnetic exchange varies from antiferromagnetic to ferromagnetic. Thus the magneto – structural correlations are expected to be interesting (**Fig. 3.7.1** to **Fig. 3.7.7**).

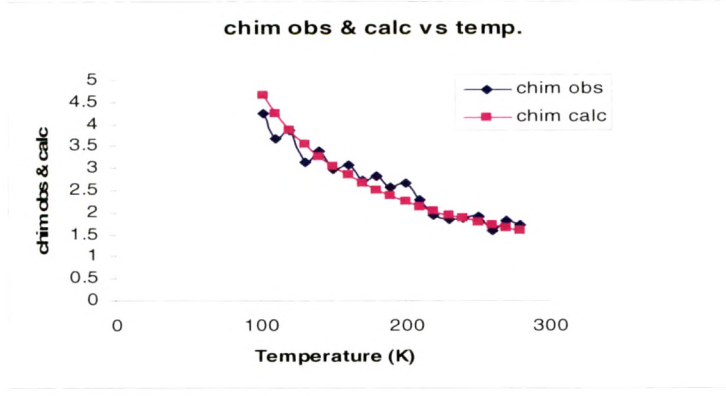

Fig. 3.7.1 $[Cu_2(bipy)_2salDPE](ClO_4)_2$

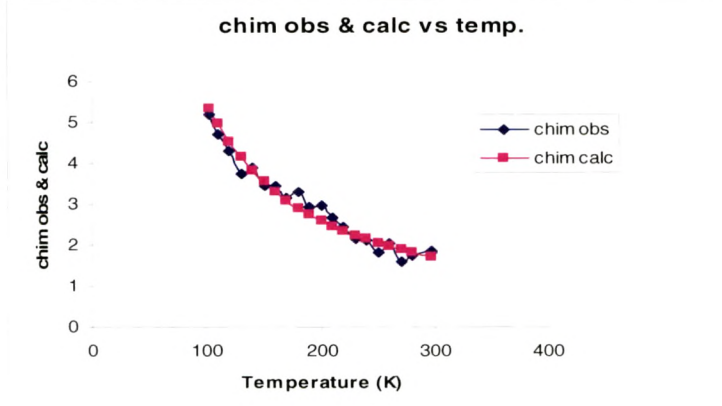

Fig. 3.7.2 $[Cu_2(bipy)_2naph3\text{-}DPS](ClO_4)_2.2H_2O$

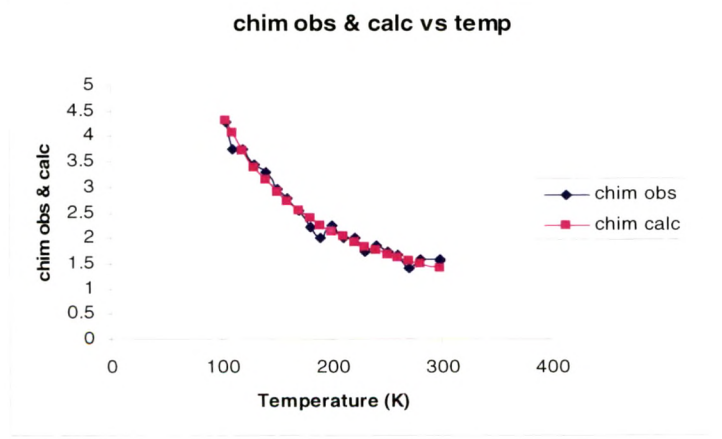

Fig. 3.7.3 $[Cu_2(phen)_2vanDPM](ClO_4)_2$

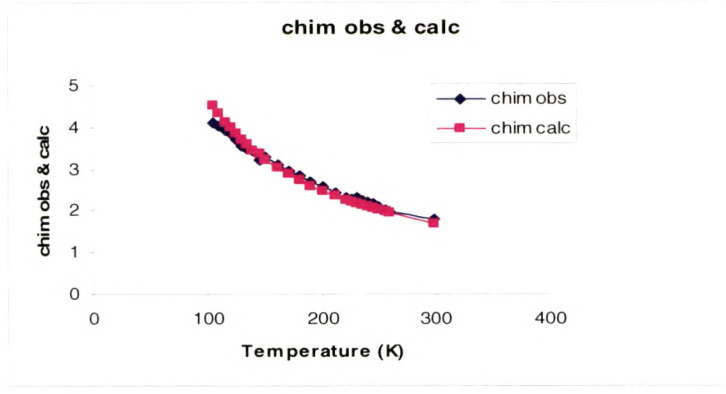

Fig. 3.7.4 $[Cu_2(bipy)_2vanDPM](ClO_4)_2$

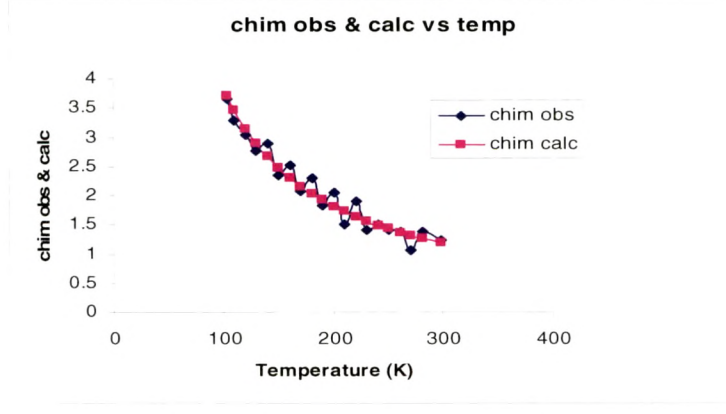

Fig.3.7.5 $[Cu_2(bipy)_2vanDPE](ClO_4)_2$.

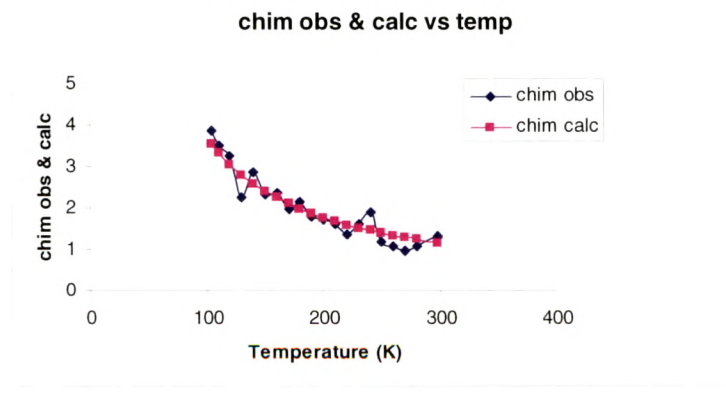

Fig.3.7.6 $[Cu_2(bipy)_2van4\text{-}DPS](ClO_4)_2$.

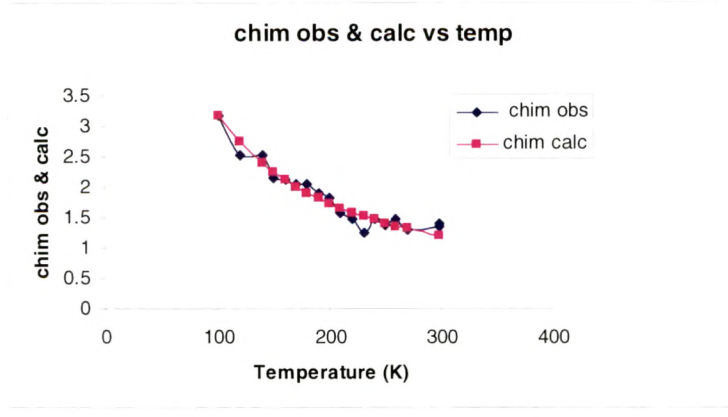

Fig.3.7.7 $[Cu_2(bipy)_2van3\text{-}DPS](ClO_4)_2$

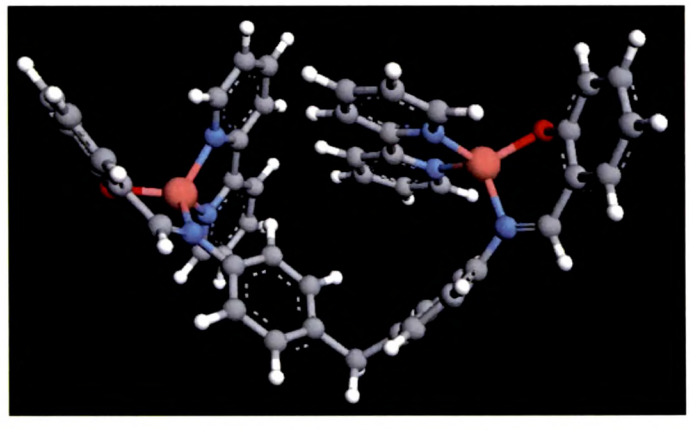

Fig.3.8.1 Optimized geometry of the binuclear complex, $[Cu_2(bipy)_2salDPM](ClO_4)_2$.

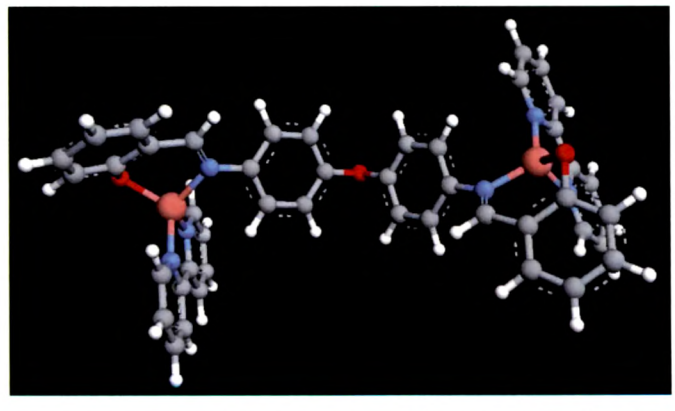

Fig. 3.8.2 Optimized geometry of the binuclear complex, $[Cu_2(bipy)_2salDPE](ClO_4)_2$.

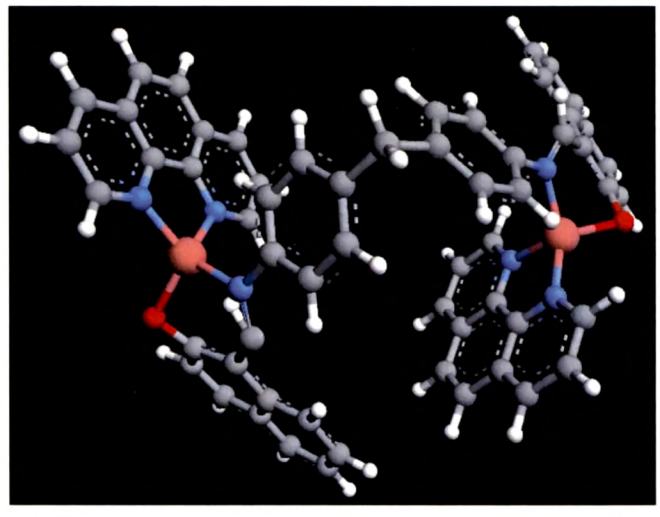

Fig. 3.8.3 Optimized geometry of the binuclear complex, $[Cu_2(phen)_2naphDPM](ClO_4)_2$.

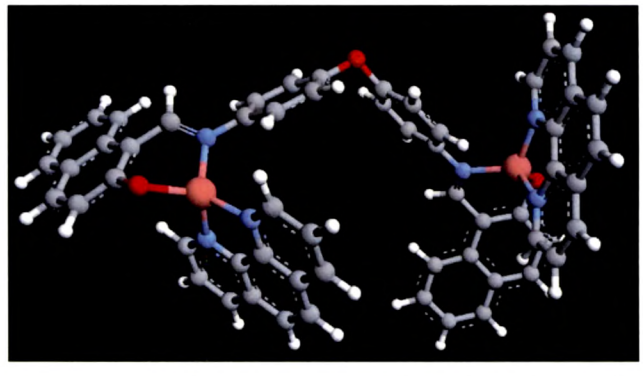

Fig. 3.8.4 Optimized geometry of the binuclear complex, $[Cu_2(phen)_2naphDPE](ClO_4)_2$.

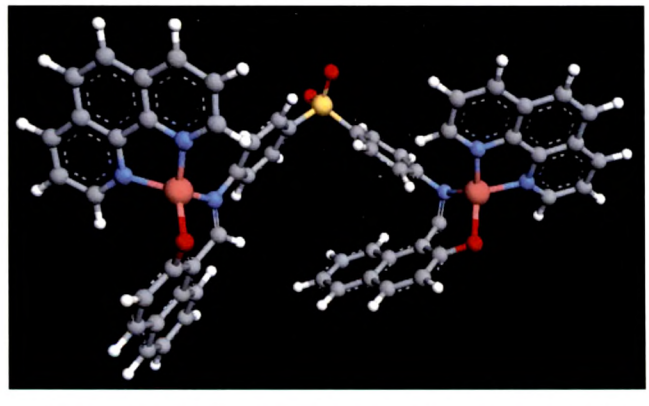

Fig.3.8.5 Optimized geometry of binuclear complex, $[Cu_2(phen)_2naph4\text{-}DPS](ClO_4)_2.2H_2O$.

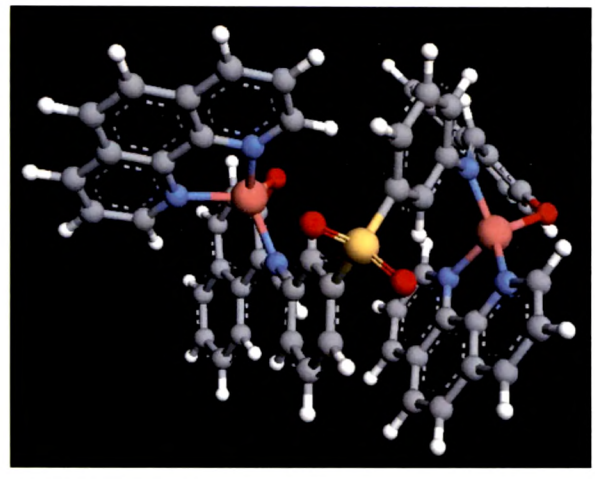

Fig. 3.8.6 Optimized geometry of binuclear complex, $[Cu_2(phen)_2naph3\text{-}DPS](ClO_4)_2.2H_2O$.

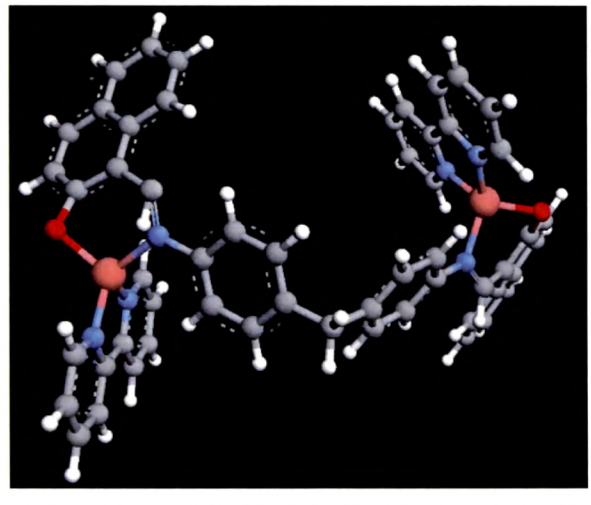

Fig. 3.8.7 Optimized geometry of binuclear complex, $[Cu_2(bipy)_2naphDPM](ClO_4)_2$.

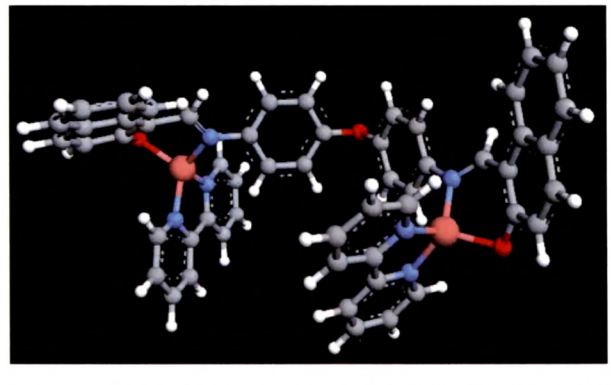

Fig. 3.8.8 Optimized geometry of binuclear complex, $[Cu_2(bipy)_2naphDPE](ClO_4)_2.2H_2O$.

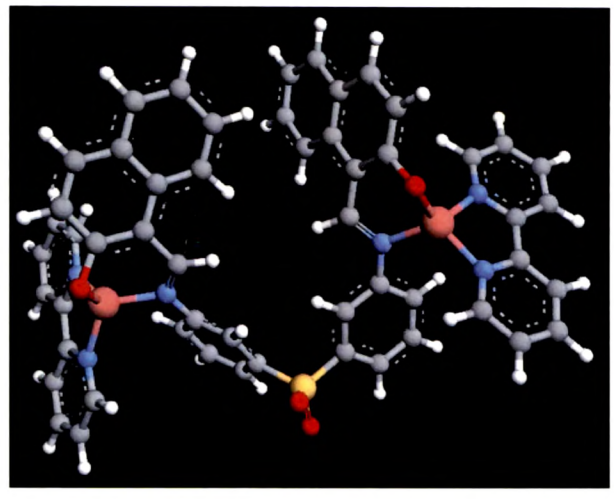

Fig. 3.8.9 Optimized geometry of binuclear complex, $[Cu_2(bipy)_2naph3\text{-}DPS](ClO_4)_2.2H_2O$.

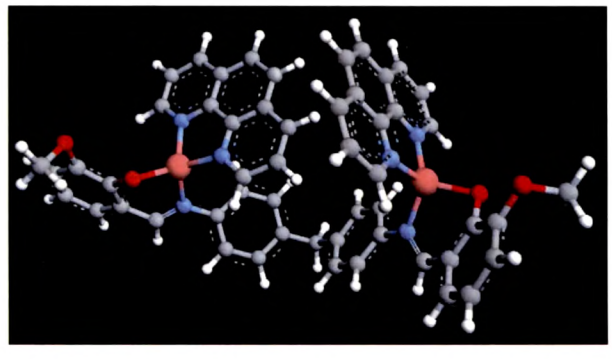

Fig. 3.8.10 Optimized geometry of binuclear complex, $[Cu_2(phen)_2vanDPM](ClO_4)_2$.

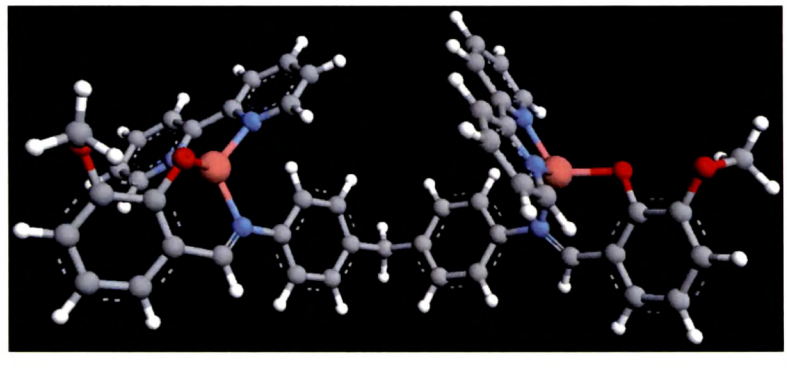

Fig. 3.8.11 Optimized geometry of binuclear complex, $[Cu_2(bipy)_2vanDPM](ClO_4)_2$.

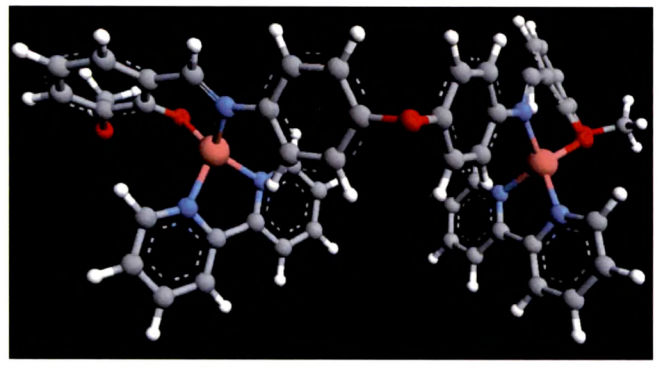

Fig. 3.8.12 Optimized geometry of binuclear complex, $[Cu_2(bipy)_2vanDPE](ClO_4)_2$.

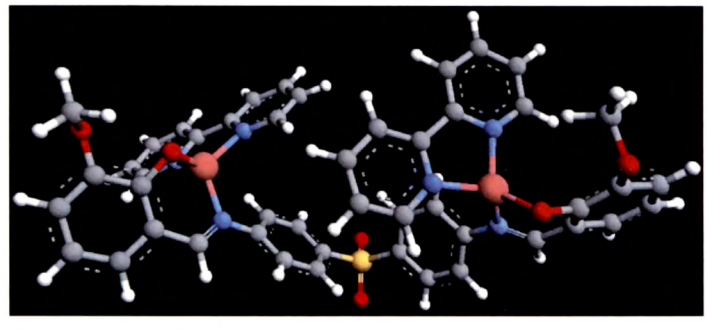

Fig. 3.8.13 Optimized geometry of binuclear complex, $[Cu_2(bipy)_2van4\text{-}DPS](ClO_4)_2$.

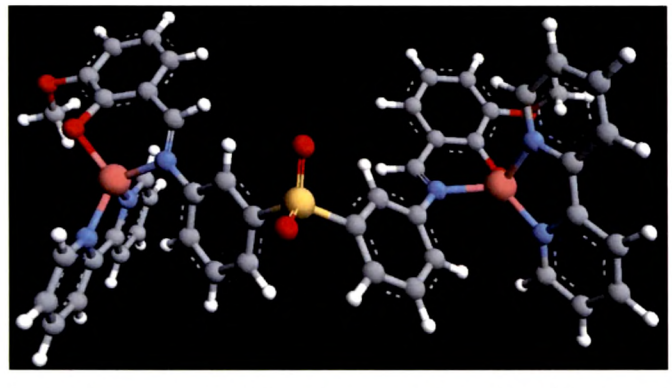

Fig. 3.8.14 Optimized geometry of binuclear complex, $[Cu_2(bipy)_2van3\text{-}DPS](ClO_4)_2$.

The complexes have very poor solubility in non coordinating solvents and hence determination of crystal structure was not possible. In order to evaluate the geometrical parameters, the geometries of the complexes were optimized using universal force field [22, 23]. Though not so accurate as quantum mechanical

calculations, it is well known that at all levels of calculations, while the absolute values of electron density, energy etc. are significantly affected, the trends and the overall geometry of the molecules remains unaltered.

The torsional angles Γ, between the metal coordination planes have been determined (**Fig. 3.8.1** to **Fig. 3.8.14**). These have been correlated with the experimentally determined J values (**Table 3.6**). Plots of J vs torsional angle Γ have been represented in **Fig. 3.9**. The series-1 corresponds to the complexes with diphenyl methane bridging, series-2, complexes with diphenyl ether bridging and series-3, 3,3'-diphenyl sulphone bridging groups. All plots of J vs torsional angle Γ show a maximum in the series of complexes with the same bridging moiety but different substitutions on non bridging part or variation in the non bridging π-bonding ligands.

Table 3.6: J, torsional angle and g values of ternary binuclear complexes.

Complexes	**J** (cm^{-1})	**Torsional angle**	**g**
$[Cu_2(bipy)_2.vanDPM](ClO_4)_2$	-9.10	100.85	2.30
$[Cu_2(bipy)_2.salDPM](ClO_4)_2$	55.00	136.15	2.00
$[Cu_2(phen)_2.vanDPM](ClO_4)_2$	52.04	148.09	1.98
$[Cu_2(phen)_2.naphDPM](ClO_4)_2.2H_2O$	29.47	164.39	1.53
$[Cu_2(bipy)_2.naphDPM](ClO_4)_2$	-1.22	166.98	2.32
$[Cu_2(phen)_2.naphDPE](ClO_4)_2.2H_2O$	-3.39	91.16	4.38
$[Cu_2(bipy)_2.salDPE](ClO_4)_2$	27.13	111.07	2.07
$[Cu_2(bipy)_2.naphDPE](ClO_4)_2.2H_2O$	68.03	116.62	1.96
$[Cu_2(bipy)_2.vanDPE](ClO_4)_2$	59.21	101.7	1.78
$[Cu_2(bipy)_2.van4\text{-}DPS](ClO_4)_2$	55.24	92.46	1.77
$[Cu_2(phen)_2.naph4\text{-}DPS](ClO_4)_2.2H_2O$	-39.89	169.54	4.69
$[Cu_2(bipy)_2.van3\text{-}DPS](ClO_4)_2$	-13.03	101.7	1.93
$[Cu_2(phen)_2.naph3\text{-}DPS](ClO_4)_2.2H_2O$	64.12	128.86	2.18
$[Cu_2(bipy)_2.naph3\text{-}DPS](ClO_4)_2.2H_2O$	57.35	159.43	2.15

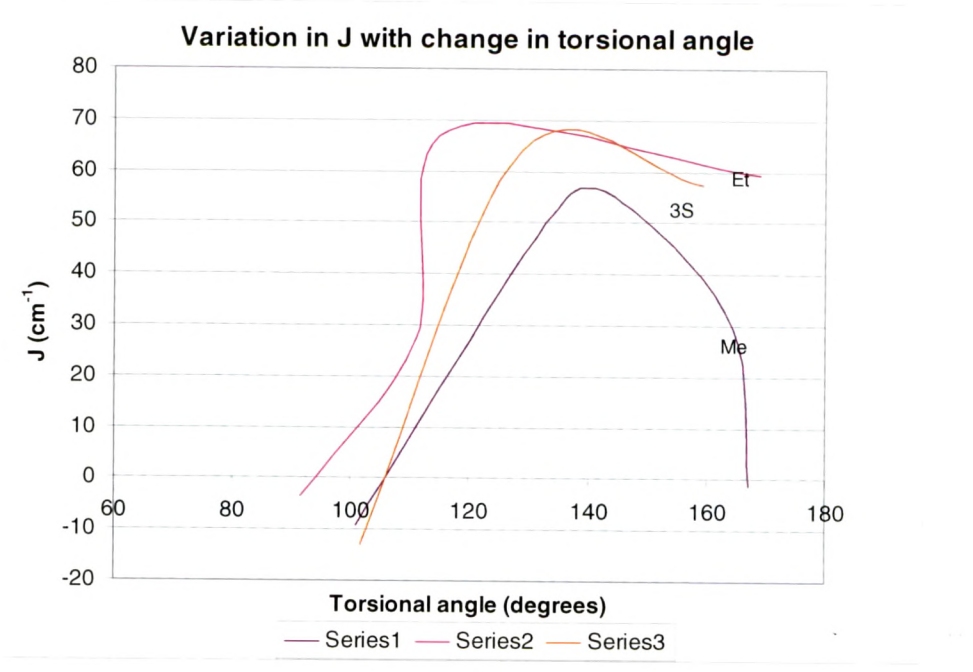

Fig. 3.9 Plot of J vs Tortional angle in binuclear complexes.

Thus, it can be concluded that a systematic variation in the non bridging part of the ligands in binuclear complexes can modulate the extent of magnetic exchange. The variation in these groups can be used to change the torsional angle and there by tune the magnetic property to any desired value from ferromagnetism to antiferromagnetism.

3.4 Reference:

[1] *"Biological and Inorganic Copper Chemistry" Eds.* K. D. Karlin and J. Zubieta, *Adenine, Guilderland, New York,1986.*

[2] E. I. Solomon, K. W. Penfield, D. E. Wilcox, *Structure Bonding, Berlin, 1983, **53**, 1.*

[3] E. I. Solomon in, 'Copper proteins' *Eds. T. G. Spiro, Wiley Interscience, New York, 1981.*

[4] H. Sigel, *Metal Ions in Biological systems, Vol. 13, Marcel Dekker, New York, 1981.*

[5] V. H. Crawford, H. W. Richardson, J. R. Wasson, D. J. Hodgson, W. E. Hatfield, *Inorg. Chem., 1976, **15**, 2107.*

[6] D. J. Hodgoson, *Prog. Inorg. Chem., 1975, **19**, 173.*

[7] W. E. Hatfield, *Comments Inorg. Chem., 1981, 1, 105.*

[8] O. Kohn, *Inorg. Chim. Acta., 1982, **62**, 3.*

[9] O. Kohn, *Comments Inorg. Chem., 1984, 3105.*

[10] M. Melnic, *Cood. Chem. Rev., 1982, **42**, 259.*

[11] M. Kato, Y. Muto, *Coord. Chem. Rev., 1988, **92**, 45.*

[12] T. R. Felthouse, E. J. Laskawski, D. N. Hendrickson, *Inorg. Chem., 1977, **16**, 1077.*

[13] C. G. Pierpont, L. C. Francesconi, D. N. Hendrickson, *Inorg. Chem., 1977, **16**, 2367.*

[14] C. G. Pierpont, L. C. Francesconi, D. N. Hendrickson, *Inorg. Chem., 1978, **17**, 3470.*

[15] C. A. Tsipis, M. P. Sigalas, V. P. Parageorgiou, M. N. Bakola – Cristino Poulou, *Can. J. Chem., 1983, **61**, 1500.*

[16] S. K. Shakhatreh, E. G. Bakalbassis, I. Brudgam, H. Hartl, J. Mrozinski, C. A. Tsipis, *Inorg. Chem. 30 (1991) 2801.*

[17] C. T. Zeyrek, A. Elmali, Y. Elerman, I. Svoboda, *Z. Naturforsch, 2005, **60b**, 143.*

[18] N. D. Kulkarni, P. K. Bhattcharya, *Can. J. Chem., 1987, **65**, 348.*

[19] K. Nakamoto, *Infrared and Raman Spectra of Inorganic and Coordination Compounds : Part B, 5th Eds, Wiley – Interscience New York (1997).*

[20] B. J. Hathaway in *Comprehensive Coord. Chem., 1987, 5, 533, Eds.,* G. Wilkinson, R. D. Gillard, J. A. Mc Cleverty, Pergamon press, Oxford.

[21] A. Bencini, D. Gatteschi, *Inorganic Electronic Structural and Spectroscopy, 1999, 1, 93, Eds.,* E. I. Solomon & A. B. P. Lever.

[22] Journal Citations for this Calculation:-

[22.a] M. A. Thompson, M. C. Zerner, *J. Am. Soc., 1991, **113**, 8210.*

[22.b] M. A. Thompson, E. D. Glendening, D. Feller, *J. Phys. Chem., 1994, **98**, 10465.*

[22.c] M. A. Thompson, G. K. Schenter, *J. Phys. Chem., 1995, **99**, 6374.*

[22.d] M. A. Thompson, *J. Phys. Chem., 1996, **100**, 14492.*

[23] UFF references:-

[23.a] A. K. Rappe, et. al., *JACS, 1992, **114**, 10024.*

[23.b] C. J. Casewit, K. S. Colwell, A. K. Rappe, *JACS, 1992, **114**, 10035.*

[23.c] C. J. Casewit, K. S. Colwell, A. K. Rappe, *JACS, 1992, **114**, 10046.*

[23.d] A. K. Rappe, W. A. Goddard, *JPC, 1991, **95**, 3358.*

[23.e] A. K. Rappe, K. S. Colwell, C. J. Casewit, *Inorg. Chem., 1993, **32**, 3438.*